Cellular/Molecular

Canonical Transient Receptor Potential 1 Plays a Role in Basic Fibroblast Growth Factor (bFGF)/FGF Receptor-1-Induced Ca^{2+} Entry and Embryonic Rat Neural Stem Cell Proliferation

Alessandra Fiorio Pla,[1] Dragan Maric,[1] So-Ching Brazer,[3] Paolo Giacobini,[2,4] Xibao Liu,[3] Yoong Hee Chang,[1] Indu S. Ambudkar,[3] and Jeffery L. Barker[1]

[1]Laboratory of Neurophysiology and [2]Cellular and Developmental Neurobiology Section, National Institute of Neurological Disorders and Stroke, and [3]Secretory and Physiology Section, Gene Therapy and Therapeutics Branch, National Institute of Dental and Craniofacial Research, National Institutes of Health, Bethesda, Maryland 20892, and [4]Department of Human and Animal Biology, University of Torino, 10123 Torino, Italy

Basic fibroblast growth factor (bFGF) and its major receptor FGF receptor-1 (FGFR-1) play an important role in the development of the cortex. The mechanisms underlying the mitogenic role of bFGF/FGFR-1 signaling have not been elucidated. Intracellular Ca^{2+} concentrations ($[Ca^{2+}]_i$) in proliferating cortical neuroepithelial cells are markedly dependent on Ca^{2+} entry (Maric et al., 2000a). The absence of voltage-dependent Ca^{2+} entry channels, which emerge later, indicates that other membrane mechanisms regulate $[Ca^{2+}]_i$ during proliferation. Canonical transient receptor potential (TRPC) family channels are candidates because they are voltage independent and are expressed during CNS development (Strübing et al., 2003).

Here, we investigated the involvement of TRPC1 in bFGF-mediated Ca^{2+} entry and proliferation of embryonic rat neural stem cells (NSCs). Both TRPC1 and FGFR-1 are expressed in the embryonic rat telencephalon and coimmunoprecipitate. Quantitative fluorescence-activated cell sorting analyses of phenotyped telencephalic dissociates show that ~80% of NSCs are TRPC1$^+$, proliferating, and express FGFR-1. Like NSCs profiled *ex vivo*, NSC-derived progeny proliferating *in vitro* coexpress TRPC1 and FGFR1. Antisense knock-down of TRPC1 significantly decreases bFGF-mediated proliferation of NSC progeny, reduces the Ca^{2+} entry component of the Ca_i^{2+} response to bFGF without affecting Ca^{2+} release from intracellular stores or 1-oleoyl-2-acetyl-*sn*-glycerol-induced Ca^{2+} entry, and significantly blocks an inward cation current evoked by bFGF in proliferating NSCs. Both Ca^{2+} influx evoked by bFGF and NSC proliferation are attenuated by Gd^{3+} and SKF96365, two antagonists of agonist-stimulated Ca^{2+} entry. Together, these results show that TRPC1 contributes to bFGF/FGFR-1-induced Ca^{2+} influx, which is involved in self-renewal of embryonic rat NSCs.

Key words: **calcium [Ca]; cortex; development; proliferation; TRPC; neural stem cells**

Introduction

Ca^{2+} is a ubiquitous second messenger, and fluctuations in cellular Ca^{2+} are critical in embryonic development (for review, see Webb and Miller, 2003). The development of the CNS initially involves extensive proliferation of cells in the neuroepithelium as uncommitted precursors divide to self-renew and generate committed progenitors, which in turn divide and differentiate into neural phenotypes. Steady-state levels of intracellular Ca^{2+} concentration ($[Ca^{2+}]_i$) in proliferating neuroepithelial cells in the embryonic rat cortex are markedly dependent on Ca^{2+} entry via unknown mechanisms (Maric et al., 2000a). The complete absence of classical voltage-dependent Ca^{2+} entry channels, which are expressed later during development, indicates that other mechanisms regulate $[Ca^{2+}]_i$ during proliferation.

Recently, Ca^{2+} entry channel proteins belonging to the canonical transient receptor potential (TRPC) family, which are voltage-independent channels (for review, see Clapham, 2003), have been identified in the embryonic rat CNS (Strübing et al., 2003). All five TRPC proteins (TRPC1, 3, 4, 5, 6) detected were more highly expressed in the embryonic CNS compared with the adult, suggesting developmental roles for TRPC channels. Heterotetramers composed of TRPC1/TRPC4/TRPC5 and TRPC1/TRPC3/TRPC6 were detected, and a role for TRPC1 expression in the formation of heterotetramers has been proposed (Strübing et al., 2003). Thus, these TRPC channels are candidates for mediating Ca^{2+} entry during proliferation of neuroepithelial cells.

Received March 15, 2004; revised Jan. 27, 2005; accepted Jan. 31, 2005.

P.G. was supported in part by Compagnia di San Paolo (Torino, Italy). We thank Dr. Craig Montell for the TRPC3 antibody. We thank Dr. Carolyn Smith, manager of the Light Imaging Facility, National Institute of Neurological Disorders and Stroke, National Institutes of Health, for support with the confocal images.

Correspondence should be addressed to either of the following: Dr. Alessandra Fiorio Pla, Laboratory of Physiology, Department of Human and Animal Biology, University of Torino, 10123 Torino, Italy, E-mail: alessandra.fiorio@unito.it; or Dr. Jeffery L. Barker, Laboratory of Neurophysiology, National Institute of Neurological Disorders and Stroke, National Institutes of Health, 36 Convent Drive, MSC 4123, Building 36, Room 4A21, Bethesda, MD 20892, E-mail: barkerj@ninds.nih.gov.

DOI:10.1523/JNEUROSCI.0951-04.2005

 0270-6474/05/252687-15$15.00/0

Recent studies have shown that TRPC1 plays a role in Ca^{2+} influx and smooth muscle cell proliferation (Golovina et al., 2001; Sweeney et al., 2002a,b) and mediates Ca^{2+} influx activated by basic fibroblast growth factor (bFGF; FGF-2) in endothelial cells (Antoniotti et al., 2002).

bFGF also plays important roles in cortical neuroepithelial cell proliferation *in vitro* and *in vivo* (Vaccarino et al., 1995, 1999a,b; Dono et al., 1998; Ortega et al., 1998; Raballo et al., 2000; Korada et al., 2002). A major receptor for bFGF, FGF receptor-1 (FGFR-1) is expressed as early as embryonic day 8.5 (E8.5) to E9.5 in the rat telencephalon, with its expression being relatively confined to the proliferating neuroepithelium (Orr-Urtreger et al., 1991; Vaccarino et al., 1999a,b). In addition, FGFR-1 expression and bFGF-mediated Ca^{2+} signaling have been detected in the majority of neural stem cells (NSC) and their proliferating progeny (Maric et al., 2003). However, the mechanisms underlying bFGF/FGFR-1 signaling in determining the various fates of NSCs including self-renewal and the role of Ca^{2+} in this process have not been studied. Furthermore, continued proliferation of cortical neuroepithelial cells *in vitro* depends on the presence of bFGF as well as physiological levels of intracellular Ca^{2+} (Ma et al., 2000).

Here, we investigate the role of TRPC1 in NSC proliferation. The results show that TRPC1 and FGFR-1 are coexpressed in the neuroepithelium, coimmunoprecipitate from extracts of telencephalic membrane preparations, and colocalize in NSC-derived proliferating progeny. Antisense knock-down of TRPC1 transcripts and proteins decrease bFGF-mediated Ca^{2+} influx, inward current responses, and proliferation of NSC progeny. Together, these results show that (1) bFGF/FGFR-1-mediated Ca^{2+} influx plays a role in embryonic rat NSC proliferation and (2) TRPC1 channels contribute to bFGF/FGFR-1-mediated Ca^{2+} influx.

Materials and Methods

Labeling of tissue sections

This research was performed in compliance with the Animal Welfare Act and the U.S. Public Health Service policy on Humane Care and Use of Laboratory Animals and was approved by the National Institute of Neurological Disorders and Stroke Animal Care and Use Committee.

FGFR1 or TRPC1 and PCNA plus Tuj1 immunostaining. Sprague Dawley rat embryos at 13 d of gestation (E13) were fixed in 4% paraformaldehyde (PF) for 4 h, cryoprotected in 30% sucrose for 3–5 d at 4°C, and frozen in dry ice. Sixteen-micrometer-thick sagittal sections were cut using a Jung Frigocut cryostat (model 2800E; Leica, Nussloch, Germany). The cells were fixed in 70% ethanol for 20 min and immunoreacted with a monoclonal mouse class IgM anti-FGFR-1 antibody (Chemicon, Temecula, CA) or a polyclonal rabbit anti-TRPC1 antibody (Wang et al., 1999) overnight at 4°C. These primary antibodies were visualized with goat anti-mouse IgM or goat anti-rabbit Alexa Fluor 546 antibodies (Molecular Probes, Eugene, OR). The cells were finally immunoreacted with a mouse monoclonal class IgG2a anti-proliferative cell nuclear antigen (PCNA; Chemicon) that labels proliferating cells and mouse monoclonal class IgG2b anti-tubulin β III antibody (Tuj1; Sigma, St. Louis, MO), which labels differentiating neurons. These reactions were visualized using goat anti-mouse IgG2a–Alexa Fluor 488 and goat anti-mouse IgG2b–Alexa Fluor 350 antibodies (Molecular Probes), respectively.

Fluorescence microscopy. Phase-contrast and fluorescence signals of cells in culture and tissue sections were imaged using an Axiovert 200 inverted fluorescence microscope (Carl Zeiss, Thornwood, NY) equipped with an Orca-ER cooled digital camera (CCD; Hamamatsu, Hamamatsu City, Japan). The cells were illuminated with a 100 W mercury arc lamp (Carl Zeiss), and the resulting fluorescence emissions were collected through a Plan-Neo 25×/0.8 oil immersion phase 2 objective (Carl Zeiss) using filter sets optimized to detect Alexa Fluor 350, Alexa Fluor 546, Alexa Fluor 488, Alexa Fluor 647, and Alexa Fluor 750 (Omega Optical, Brattleboro, VT). Fluorescence emissions for each fluorochrome signal were captured separately as a 12-bit image, using the video sensor of the Orca-ER camera at a 512 × 480 pixel resolution, and analyzed using Adobe Photoshop software (Adobe Systems, San Jose, CA). In some experiments, fluorescence microscopy was used to quantify the fluorescence intensity of individual cells from 10 fields selected randomly from TRPC1 antisense-treated and random oligonucleotide (ODN)-treated cells, which served as a control. OpenLab software (Improvision, Lexington, MA) was used to acquire and analyze the images. For each set of experiments, identical settings of the OpenLab system were used. The cells were outlined manually, and the mean fluorescence intensity was obtained for the delineated regions. Data are presented as relative fluorescence intensity in arbitrary units. For confocal analyses, cells were imaged with an LSM 510 inverted fluorescence microscope (Carl Zeiss), and the resulting fluorescence emissions were collected through a 63×, 1.4 numerical aperture oil immersion objective (Carl Zeiss). Alexa Fluor 488 (Molecular Probes) fluorescence signals of individual cells were excited by an argon–ion laser at 488 nm, and Alexa Fluor 546 (Molecular Probes) fluorescence signals of individual cells were excited by an argon–ion laser at 543 nm.

Labeling of cells in suspension

Surface epitope labeling for cell identification. E13 telencephalic cells were identified using lineage-specific surface markers, as described previously (Maric et al., 2003). Briefly, the tissues were optimally dissociated into single-cell suspensions with papain (Maric et al., 1997, 1998a). Neuroglial and oligodendrocyte type 2 astrocyte oligoglial progenitors were immunoidentified using anti-A2B5 (Chemicon) and JONES (Sigma) antibodies and optimally visualized with an appropriate phycoerythrin (PE)-conjugated secondary antibody (Caltag, Burlingame, CA). Neuronal progenitors and differentiating neurons were labeled with cholera toxin B subunit (ChTx; Sigma) and tetanus toxin fragment C (TnTx; Roche Diagnostics, Indianapolis, IN) and visualized using appropriate PE/carbocyanine dye 5 (CY5)-conjugated secondary reagents (Caltag). Annexin V (Trevigen, Gaithersburg, MD), which was visualized with PE/Texas Red (TR)-conjugated secondary reagent, was used as an additional surface marker in conjunction with forward angle light scatter, a property related to cell size, to discriminate among apoptotic, necrotic, and nonapoptotic cells (data not shown) (Maric et al., 2003).

Colabeling of surface-phenotyped cells for expressions of FGFR-1 and PCNA or TRPC1. After surface immunophenotyping (see above), E13 telencephalic cells were then double-fixed first in 4% PF for 20 min at room temperature, followed by 70% ethanol for 20 min at room temperature, and washed in Dulbecco's PBS (Quality Biological, Gaithersburg, MD) supplemented with 1 mg/ml bovine serum albumin (BSA). The cells were immunoreacted with rabbit anti-FGFR-1 antibody (Santa Cruz Biotechnology, Santa Cruz, CA) and mouse IgG2a anti-PCNA antibody (Chemicon) for 1 h at room temperature, and these reactions were then visualized with Alexa Fluor 350-conjugated goat anti-rabbit and fluorescein isothiocyanate (FITC)-conjugated goat anti-mouse IgG2a antibodies (Caltag). In another set of experiments, after immunophenotyping and double-fixation (see above), the cells were immunoreacted with rabbit anti-TRPC1 antibody (Wang et al., 1999) and the reaction was visualized with FITC-conjugated donkey anti-rabbit IgG secondary antibody (Jackson ImmunoResearch, West Grove, PA). This multistaining protocol revealed the distribution of FGFR-1 and TRPC1 among the proliferating ($PCNA^+$) and nonproliferating ($PCNA^-$) cells in each phenotyped population.

Quantitative flow cytometric analysis. The fluorescent labeling reactions of cells in suspension were analyzed using a FACSVantage SE flow cytometer (Becton Dickinson, Mountain View, CA) equipped with three lasers, which provide excitation wavelengths tuned to 488 nm, 647 nm, and broad UV (351–364 nm). The FITC and PE, PE/TR, and PE/CY5 fluorescence signals of individual cells were excited by an argon–ion laser at 488 nm, and the resulting fluorescence emissions from each cell were collected using bandpass filters set at 530 ± 30, 575 ± 25, 613 ± 20, and 675 ± 20 nm, respectively. Alexa Fluor 350 was excited using a UV laser, and its emission was collected through 424 ± 22 nm bandpass filter. Cell

Quest Acquisition and Analysis software (Becton Dickinson) was used to acquire and quantify the fluorescence signal intensities and to graph the data either as single-parameter histograms or bivariate dot density plots. In multiple labeling experiments, fluorescence emissions of individual fluorophores were corrected for spectral overlap using electronic compensation.

Protein extraction and Western blot analysis

Telencephalic tissue from E13 embryos was dissected and homogenized with a Dounce homogenizer, diluted in lysis buffer (100 mM Tris-HEPES, pH 8.0, and 1 mM $MgCl_2$) supplemented with protease inhibitor mixture (Roche Molecular Biochemicals, Indianapolis, IN), and centrifuged at 30,000 × *g* for 1 h to obtain the heavy membrane fraction that was frozen and stored at −80°C until further use. Protein concentration was determined using protein assay solution (Bio-Rad, Hercules, CA). Conditions for SDS-PAGE and Western blotting were as described previously (Wang et al., 1999). Polyvinylidene difluoride membranes were blocked and incubated for 1 h with rabbit IgG anti-TRPC1 antibody (Wang et al., 1999) and rabbit IgG anti-FGFR-1 antibody (Santa Cruz Biotechnology). As a control, the membrane fraction was incubated with anti-TRPC1 in the presence of the corresponding antigen peptide (1 mg). The membrane was washed with Tris-buffered saline containing 0.1% Tween 20, incubated as required with HRP-conjugated anti-rabbit IgG antibody (Jackson ImmunoResearch), washed, treated with Super Signal West Pico chemiluminescent substrate (Pierce, Rockford, IL), and exposed to X-Omat films (Eastman Kodak, Rochester, NY).

Detergent solubilization of cell membranes and immunoprecipitation

Telencephalic tissue from E13 embryos was dissected and homogenized with a Dounce homogenizer, diluted in sucrose buffer (0.25 M sucrose and 10 mM Tris-HEPES, pH 7.4) supplemented with protease inhibitor mixture (Roche Molecular Biochemicals), and centrifuged at 100,000 × *g* for 1 h to obtain a microsome fraction. Solubilization and immunoprecipitation were performed with an octyl glucoside (OG) and potassium iodide (KI) solubilized preparation of the E13 telencephalic microsome fraction, as described previously (Lockwich et al., 2001). Briefly, 2 mg of the microsome fraction was washed by dilution into 5–6 ml of a buffer containing (in mM) 200 KCl, 50 K-4-morpholinepropanesulfonic acid (MOPS), pH 7.5, 2.5$MgCl_2$, and 1 4-(2-aminoethyl) benzenesulfonylfluoride (AEBSF), followed by centrifugation at 50,000 × *g* for 30 min. The washed membranes were solubilized with 1.5% OG (Calbiochem, La Jolla, CA) in 0.96 ml of a medium containing 50 mM K-MOPS, pH 7.5, 20% (v/v) glycerol, 0.5 M KI, 1.5 mM $MgCl_2$, 1 mM dithiothreitol, 0.5 mM AEBSF, 0.167 mM pepstatin A, 0.167 mM leupeptin, and 10 mg of lipids (Avanti Polar Lipids, Alabaster, AL) from a 50 mg/ml aqueous stock suspension containing 2% (v/v) β-mercaptoethanol (Sigma). The lipid stock solution consisted of 60% *Escherichia coli* ether-washed bulk lipids, 17.5% phosphatidylcholine, 10% phosphatidylserine, and 12.5% cholesterol. The detergent-treated membranes were incubated on ice for 20 min and then centrifuged for 1 h at 145,000 × *g*. OG and KI solubilized fractions of the E13 telencephalic microsome fraction were incubated with anti-TRPC1 antibody (1:20 dilution) overnight, then pulled down with precleaned protein A-Sepharose CL-4B beads (50 mg/ml; Amersham Biosciences, Piscataway, NJ). The immunoprecipitated proteins were recovered by centrifugation for 1 min at 1000 × *g*. The beads were washed three times with buffer containing 500 mM NaCl, 10 mM Tris-HCl, pH 7.5, 10% (w/v) sucrose, 1 mM EDTA, 0.2 mM sodium vanadate, 0.2 mM phenylmethylsulfonyl fluoride, 0.5% (v/v) Nonidet P-40 (Sigma), 1 μg/ml aprotinin, 1 μg/ml leupeptin, and 1 μg/ml pepstatin A. The washed beads were then incubated with 200 μl of SDS-PAGE sample buffer for 5 min at 95°C. The immunoprecipitated proteins (and coimmunoprecipitated proteins) were detected by SDS-PAGE followed by Western blotting, as described above.

Cell sorting

We used E13 telencephalic tissues as a primary source of NSCs for fluorescence-activated cell sorting (FACS) and experimentation *in vitro*. The methods are, for the most part, based on a recently published strategy (Maric et al., 2003). After dissociation, the cells were then labeled with antibodies against surface markers identifying early neuronal and/or glial progenitors (detailed briefly above) (see Fig. 2*A1*). Vital NSCs were then physically purified using a FACSVantage SE flow cytometer (Becton Dickinson) in conjunction with a quintuple epitope-negative selection sorting protocol (Maric et al., 2003). During the initial cell preparation, labeling of surface epitopes, and FACS, the cells were maintained in a normal physiological medium (NPM) supplemented with 1 mg/ml BSA. NPM consisted of the following (in mM): 145 NaCl, 5 KC1, 1.8 $CaCl_2$, 0.8 $MgCl_2$, 10 glucose, and 10 HEPES (all from Sigma), with pH and osmolarity adjusted to 7.3 and 290 mOsm, respectively.

Cell culture

Sort-purified NSCs were plated at clonal cell densities (5×10^3 cells/cm^2) on poly-D-lysine (Sigma)- and bovine plasma fibronectin (Invitrogen, Frederick, MD)-coated coverslips, which were photo-etched with an alphanumeric grid (Bellco Glass, Vineland, NJ) and preglued to 35 mm tissue culture dishes (MatTek, Ashland, MA). Clones derived from isolated cells were followed over a 7 d period using an Axiovert 200 inverted microscope (Carl Zeiss). The cells were cultured under control conditions in Neurobasal medium (Invitrogen) supplemented with 1× working stock of B27 additives (diluted 50-fold from commercially available stock; Invitrogen) and 10 ng/ml human recombinant bFGF (Intergen, Purchase, NY). Experimental plates of cells were treated with TRPC1 antisense or missense ODNs, or with antagonists of voltage-independent Ca^{2+} channels (SKF96365, Gd^{3+}; Sigma), or L-type voltage-dependent Ca^{2+} channels (nitrendipine; Sigma).

Labeling and quantitative analysis of cells in culture

FGFR1 and TRPC1. Cells in culture were double-fixed in PF and ethanol, as described above, and immunoreacted with a polyclonal rabbit IgG anti-TRPC1 antibody (Wang et al., 1999), a mouse monoclonal class IgM anti-FGFR-1 antibody (Chemicon), a mouse monoclonal class IgG1 anti-vimentin antibody (Chemicon), which labels immature precursors and progenitors, and a mouse monoclonal class IgG2a anti-PCNA antibody. The reactions were visualized with goat anti-rabbit IgG–Alexa Fluor 546, goat anti-mouse IgM–Alexa Fluor 488, and goat anti-mouse IgG1–Alexa Fluor 350 antibodies (Molecular Probes), respectively. PCNA immunoreaction was visualized with biotinylated goat anti-mouse IgG2a antibody (Caltag), followed by Alexa Fluor 750-conjugated streptavidin (Molecular Probes).

Multi-epitope staining for proliferation and differentiation. The cells were first surface-immunoreacted with a mouse monoclonal class IgM JONES antibody (Sigma), followed by goat-anti mouse IgM–Alexa Fluor 350 antibody (Molecular Probes), and then sequentially double-fixed in PF and ethanol. The same cells were subsequently probed for lineage-specific cytoskeletal markers, including a mouse monoclonal class IgG1 anti-vimentin antibody (Chemicon), a mouse monoclonal class IgG2b anti-Tuj1 antibody. These immunoreactions were visualized with a biotinylated goat anti-mouse IgG1 antibody (Caltag), followed by Alexa Fluor 750-conjugated streptavidin (Molecular Probes) and a goat anti-mouse IgG2b–Alexa Fluor 647 antibody (Molecular Probes), respectively. The cells were finally probed for nuclear markers, including a proliferation-selective mouse monoclonal class IgG2a anti-PCNA antibody (Chemicon) and a total DNA stain (Sytox Orange; Molecular Probes). PCNA immunoreaction was visualized with goat anti-mouse IgG2a–Alexa Fluor 488 antibody (Molecular Probes). Sytox Orange was used to count the total cell number and to discriminate between viable cells and those undergoing apoptotic (fragmented nuclei) or necrotic (pyknotic nuclei) cell death.

In optimizing the above protocols, we have performed all of the appropriate control experiments to confirm the specificity of each immunoreagent. Control immunoreactions using single-, double-, or triple-staining protocols revealed no significant cross-epitope immunoreactivity among primary or secondary antibodies.

Reverse transcription-PCR

Total RNA was isolated from sort-purified NSC progeny, which had been treated with either TRPC1 antisense or control ODNs (see below) for 7 d in culture, using RNA STAT-60 (Tel-Test, Friendswood, TX) following the manufacturer's protocol. Briefly, cells were homogenized (1 ml of

Table 1. ODN sequences of primers used for RT-PCR

Primers	Oligo	Sequence (5′–3′)
TRPC1	Forward	cttgtcaccaggtttagctatgggg
	Reverse	gcaagatcttggcgcagttcattgag
TRPC2	Forward	cgttccagtttctctttctggaccat
	Reverse	agcatcgtcctcgatcttctgg
TRPC3	Forward	tgacttccgttgtgctcaaatatg
	Reverse	tctgaagccttctccttctgc
TRPC4	Forward	tggcgtctcgctggtac
	Reverse	aggacccacggtaatatc
TRPC5	Forward	gtactgctggcttttgcc
	Reverse	ttcagcagcactaccagg
TRPC6	Forward	tcatcatggtgtttgtggc
	Reverse	gcaaaacaatgaccattgtaa
TRPC7	Forward	agtacgtgctgcacttgtgg
	Reverse	gagatgatctgggggtctga
L-19	Forward	cctgaaggtcaaagggaatgtgttc
	Reverse	ggacagagtcttgatgatctcctcc

RNA STAT-60/50–100 mg), chloroform was added (0.2 ml/ml homogenate), and the mixture was spun. To the aqueous layer, isopropanol was added (0.5 ml) to precipitate RNA. The RNA pellet was washed (75% ethanol), air dried, and resuspended (DEPC-treated water). One microgram of each sample was used for reverse transcription (RT)-PCR.

First-strand cDNAs were synthesized using the SuperScript III First-Strand Synthesis System for RT-PCR (Invitrogen) following the manufacturer's instructions.

PCR was performed to detect the different *TRPC* channel transcripts and the 60S ribosomal subunit gene, *L-19*. PCR primer pairs are reported in Table 1 . All designed primers were screened using BLAST (Basic Local Alignment Search Tool) to ensure specificity of binding. Primers were used at a concentration of 250 nM.

For each reaction, 30.5 μl of nuclease free H_2O, 5 μl of 10× PCR GOLD buffer (Applied Biosystems, Foster City, CA), 4 μl of 25 mM $MgCl_2$, 5 μl of deoxynucleoside triphosphate mix (2.5 mM), and 0.5 μl of Amplitaq Gold (Applied Biosystems) were mixed. Primers (2 μl of each) and template cDNA (2 μl) were added to the mixture. The PCR program was as follows: 10 min 94°C pre-run, 30 s at 94°C, 30 s at 55°C, 2 min at 72°C for 35 cycles, and 10 min 72°C post-run. No products were amplified in water.

Antisense targeting

Phosphorothionate-modified TRPC1 ODNs (5′-TGCTCCTTTGAAGTATATCCTTTA-3′) were synthesized and purified by Biognostick (Göttingen, Germany). The control, provided by Biognostik, was a GC-matched randomized-sequence ODN (missense). Cells were grown on glass coverslips for 7 d in the presence of 2 or 5 μM antisense/TRPC1 or control ODNs and then examined for downregulation of TRPC1 transcript expression by RT-PCR, as described above. For analyses of different TRPC protein expressions, single-cell staining immunofluorescence was performed using polyclonal rabbit IgG anti-TRPC1 (Wang et al., 1999), chicken TRPC3 antisera (a kind gift from Dr. C. Montell, Departments of Biological Chemistry and Neuroscience, Johns Hopkins University School of Medicine, Baltimore, MD), rabbit IgG anti-TRPC4 (Chemicon), and IgG anti-TRPC6 (Sigma) antibodies at a 1:100 dilution factor. The stainings were revealed with goat anti-rabbit IgG–Alexa Fluor 546 (Molecular Probes) and with anti-chicken FITC-conjugated (Jackson ImmunoResearch) antibodies. In other sets of experiments, NSC progeny grown for 7 d in culture in the presence of TRPC1 antisense or control ODN were used for Ca^{2+} imaging, electrophysiological recordings, or multi-epitope staining for proliferation and differentiation, as described above.

Calcium imaging

Changes in $[Ca^{2+}]_i$ levels in cultured cells were measured according to methods described previously (Maric et al., 2000b,c, 2003). Briefly, the cells were loaded with fura-2 AM and imaged at 2 s intervals using the Attofluor RatioVision workstation (Atto Bioscience, Rockville, MD). All recording solutions were warmed to 37°C and delivered to the 150 μl recording chamber using gravity-driven perfusion at a constant flow rate of ~2 ml/min.

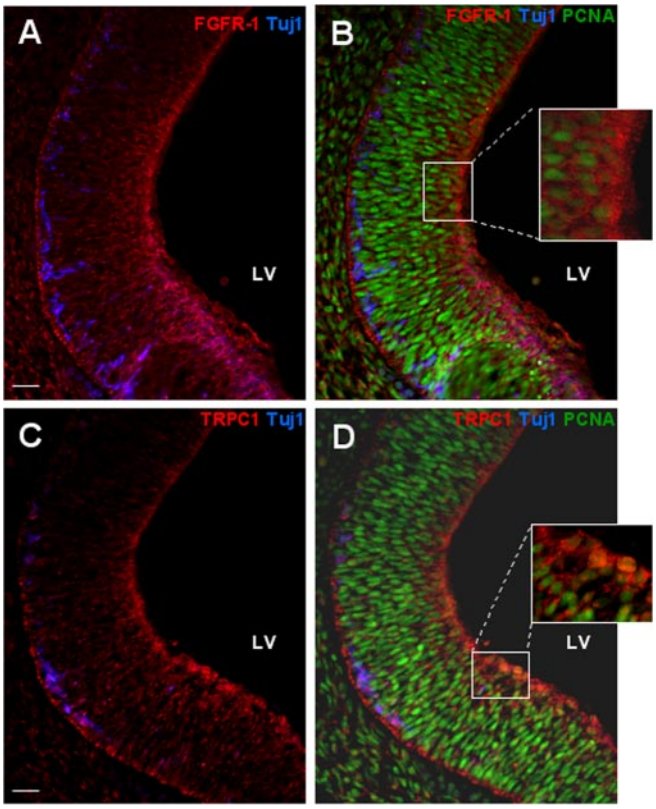

Figure 1. TRPC1 and FGFR-1 are expressed by proliferating neuroepithelial cells in the E13 rat telencephalon. ***A***, ***B***, After fixation, sagittal sections of the E13 brain were immunostained for FGFR-1 (red), Tuj1 (blue), and PCNA (green). FGFR-1 is present throughout the neuroepithelium and is coexpressed with proliferating ($PCNA^+$) cells along the LV. ***C***, ***D***, E13 sections were fixed and stained for TRPC1 (red), Tuj1 (blue), and PCNA (green). TRPC1 expression is more restricted to cells near the LV and, like FGFR-1, is coexpressed in $PCNA^+$ cells lining the LV surface. The insets are magnified regions of the boxed areas. Scale bar, 10 μm.

Electrophysiological recordings

For patch-clamp experiments, coverslips of NSCs cultured for 7 d in antisense/TRPC1 or missense were transferred to the recording chamber and kept in a Ringer's solution of the following composition (in mM): 145 NaCl, 5 KCl, 1 $MgCl_2$, 1 $CaCl_2$, 10 HEPES, and 10 glucose, pH 7.4 (NaOH). The patch pipettes had resistances of 3–5 MΩ after filling with the standard intracellular solution that contained the following (in mM): 145 Cs methane-sulfonate, 8 NaCl, 10 $MgCl_2$, 10 HEPES, and 10 EGTA, pH 7.2 (CsOH). External solutions were composed as follows (in mM): 145 NaCl, 5 CsCl, 1 $MgCl_2$, 10 $CaCl_2$, 10 HEPES, and 10 glucose, pH 7.4 (NaOH). A divalent cation-free (DVF) solution contained the following (in mM): 165 NaCl, 5 CsCl, 10 EDTA, 10 HEPES, and 10 glucose, pH 7.4 (NaOH). An *N*-methyl-D-glucamine (NMDG) solution contained the following (in mM): 170 NMDG, 5 CsCl, 1 $MgCl_2$, 10 HEPES, and 10 glucose, pH 7.4 (HCl). The osmolality for all of the solutions was adjusted with mannose to 300–315 mmol/kg using a Vapor Pressure Osmometer (Wescor, Logan, UT).

Patch-clamp experiments were performed in the tight-seal whole-cell configuration at room temperature (22–25°C) using an Axopatch 200B amplifier (Axon Instruments, Union City, CA). The cells were routinely held at 0 mV, and the development of a current in response to bFGF was assessed by measuring the current amplitudes at a potential of −80 mV, taken from high-resolution currents in response to voltage ramps ranging from −90 to 90 mV over a period of 1 s every 4 s and digitized at a rate of 1 kHz. This electrophysiological protocol has been applied previously

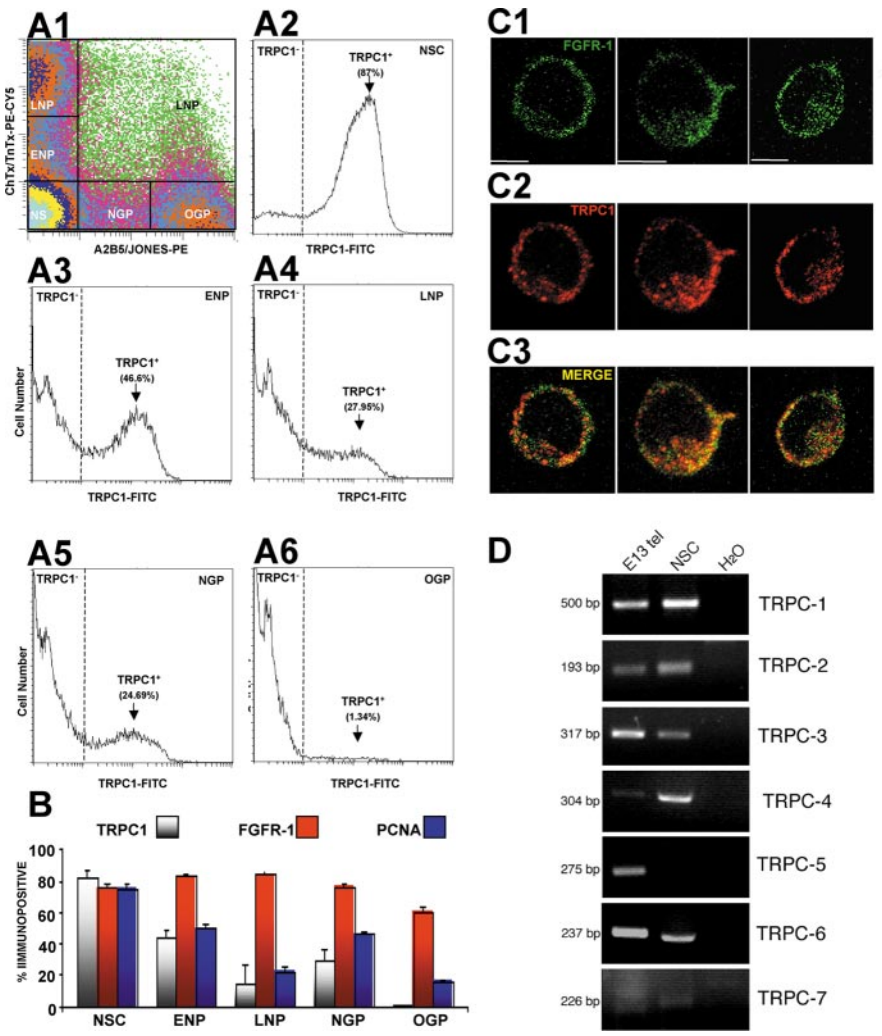

Figure 2. TRPC1, FGFR-1, and PCNA distributions among phenotyped E13 telencephalic cells and coexpression of TRPC1 transcripts with other TRPCs in NSCs. Dissociates of the E13 rat telencephalon were phenotyped *ex vivo* using surface markers for neuronal progenitors (ChTx, TnTx), neuroglial progenitors (A2B5, JONES), and apoptotic cells (annexin V) (data not shown), fixed, and immunoreacted to reveal their proliferation (PCNA) status and their expression of either TRPC1 or FGFR-1 (data not shown). The complex distribution of labeling reactions was quantified by FACS and displayed as dot density plots in pseudocolor to reveal the conjoint distributions of fluorescence signals reflecting extracellular and intracellular epitopes and the percentages of cells expressing them. ***A1***, Surface labeling with differentiating markers identifies six cell populations composing E13 telencephalic dissociates that include NSCs, which are devoid of the distinguishing surface markers, neuroglial progenitors (NGP), oligoglial progenitors (OGP), ENPs, and two populations of late neuronal progenitors (LNP, which are ChTx$^+$TnTx$^+$A2B5$^-$JONES$^-$, and quadruple-positive cells, which are ChTx$^+$TnTx$^+$A2B5$^+$JONES$^+$). The boxed regions represent electronic FACS gates used to identify and quantify individual populations. ***A2–A6***, Frequency histograms demonstrate the relative numbers of TRPC1$^+$ cells in the five subpopulations identified in ***A1***. ***B***, Bar plot summarizes the relative abundance of TRPC1$^+$ (gray bars), FGFR-1$^+$ (red bars), and PCNA$^+$ (blue bars) cells in each of the five populations. The percentages of TRPC1$^+$ and PCNA$^+$ cells are greatest among NSCs and decline as cells differentiate along neuronal and neuro-/oligoglial lineages. FGFR-1$^+$ cells are widely distributed throughout the populations. Data are means ± SEM of three independent experiments. ***C1–C3***, Confocal images of three representative NSCs show cellular localizations of TRPC1 (***C1***) and FGFR-1 (***C2***) in freshly sorted cells acutely cultured for 1 h. ***C3***, Merge of ***C1*** and ***C2*** shows the colocalization of TRPC1 (red) and FGFR-1 (green) as a yellow signal. Color-coded epitopes are identified in each panel. Scale bar, 10 μm. ***D***, PCR analysis of different TRPC mRNAs in E13 telencephalic dissociates (E13 tel) and in the freshly sorted NSC population (NSC). Equal amounts of RNA were reversed transcribed to generate cDNA. The cDNA was subjected to PCR amplification using paired primers specific for the different TRPCs. The right lane shows the negative control for each paired primer set used (H_2O). NSCs clearly express TRPC1–4 and TRPC6, whereas the telencephalic dissociates express these and TRPC5. TRPC7 is barely detectable in NSCs.

to study Ca^{2+}-permeable cation currents in other cell types (Liu et al., 2004). A liquid-junction potential, which was <8 mV, was not corrected, and capacitative currents and series resistance were determined and minimized. For analysis, the first ramp obtained under baseline conditions was used for leak subtraction of the subsequent current–voltage (*I–V*) plots.

Statistical analysis

One-way ANOVA was performed to analyze sets of data. *Post hoc* tests were used to determine statistically significant differences among the groups (Student's *t* test). Data were considered significantly different if $p < 0.05$. All data are expressed as means ± SEM.

Results

Differential distributions of FGFR-1 and TRPC1 in the developing telencephalon

Immunohistochemistry was performed to reveal the distributions of FGFR-1 and TRPC1 immunoreactivities in the embryonic telencephalon at the beginning of neurogenesis. FGFR-1 was primarily distributed in cells lining the lateral ventricle (LV), although some signal was also apparent in the neuroepithelium away from the ventricle (Fig. 1*A*). This is consistent with previous studies (Raballo et al., 2000). Immunostaining with anti-tubulin β III antibody (Tuj1), which labels differentiating neurons, showed the distributions of neuronal progenitors and postmitotic neurons in the telencephalon (Fig. 1*A*). Some of the FGFR-1 immunoreactivity was expressed by cells progressing along the neuronal lineage. Tissue sections were also immunostained for the presence of PCNA to reveal the distribution of proliferating precursors and progenitors. FGFR-1 was detected in PCNA$^+$ cells primarily at the interface with the LV (Fig. 1*B*). These results show that FGFR-1 is widely distributed in the proliferating neuroepithelium. Unlike the broad distribution of FGFR-1, TRPC1 was predominantly confined to the cells lining the LV (Fig. 1*C*) and was coexpressed with proliferating (PCNA$^+$) elements (Fig. 1*D*). In addition, TRPC1 and FGFR-1 signals were found to be colocalized in individual cells interfacing with the LV (data not shown). Together, these results reveal that FGFR-1 and TRPC1 are coexpressed in proliferating neuroepithelial cells.

Distributions of TRPC1, FGFR-1, and PCNA expressions among phenotyped telencephalic cells

We used multi-epitope immunophenotyping of telencephalic dissociates in conjunction with FACS to quantify the distributions of TRPC1 and FGFR-1 among proliferative (PCNA$^+$) NSCs and committed neuronal and neuro-/oligoglial progenitors. NSCs were identified by their lack of four surface ganglioside markers (ChTx$^-$TnTx$^-$A2B5$^-$JONES$^-$), which emerge as NSCs differentiate into progenitor phenotypes, whereas different progenitors were identified by their specific patterns of ganglioside expression (Fig. 2*A1*) (Maric et al., 2003). Each subpopulation was further divided into vital

(nonapoptotic) and apoptotic cells by their expression of annexin V binding to phosphatidylserine residues at the cell surface (data not shown). The results show that the great majority (~80%) of NSCs expressed TRPC1 (Fig. 2*A2*), which progressively decreased in abundance during both neuronal and neuro-/oligolgial lineage progressions (Fig. 2*A3–A6*). Oligolgial progenitors were virtually devoid of TRPC1$^+$ cells, whereas a minority of "late" or well advanced neuronal progenitors expressed TRPC1 (Fig. 2*A3–A6*,*B*). Most TRPC1$^+$ NSCs coexpressed PCNA (Fig. 2*B*), consistent with the coexpression of TRPC1 in PCNA$^+$ cells *in vivo* (Fig. 1*D*). Both TRPC1 and PCNA expression proportionately decreased as NSCs progressed along the neuronal lineage. About one-half of the newly committed neuronal progenitors were TRPC1$^+$ PCNA$^+$, whereas ~15–20% of the more differentiated progenitors were double positive (Fig. 2*B*). Both TRPC1$^+$ and PCNA$^+$ cells also decreased during neuro-/oligoglial lineage progression (Fig. 2*B*). The coexpression of TRPC1 and PCNA among NSCs and neuroglial and neuronal progenitor cells demonstrate that the channel is specifically present in cells that are actively proliferating rather than in cells that are preterminally or terminally postmitotic.

Immunophenotyped populations were also probed for FGFR-1 expression in the context of PCNA staining. FGFR-1 and PCNA signals were highly coexpressed in NSCs (data not shown) (results plotted in Fig. 2*B*). Thus, NSCs actively proliferating *in vivo* express both TRPC1 and FGFR-1. However, whereas TRPC1$^+$PCNA$^+$ cells decreased during cell lineage progression, FGFR-1 immunoreactivity could be detected in the great majority of differentiating cells. This reveals that FGFR-1 persists in preterminally and terminally postmitotic cells.

Confocal microscopy was used to resolve the localization of TRPC1 and FGFR1 in single cells. NSCs, sorted as described above, were plated and allowed to attach for 1 h. Cells were then fixed in 4% PF and stained for FGFR-1 and TRPC1. No detergent was used to permeabilize the cells. The data show that TRPC1 and FGFR-1 were expressed in the plasma membrane region, as well as intracellularly (Fig. 2*C1*,*C2*). A similar intracellular localization for TRPC1 has been described previously in human salivary gland (HSG) cells (Brazer et al., 2003). Notably, in another study, a considerable amount of TRPC1 appeared to be localized intracellularly in hippocampal neurons, and the presence of TRPC1 in the surface membrane fraction was detected by biotinylation (Bezzerides et al., 2004). In NSCs, colocalization of TRPC1 and FGFR-1 can be detected as a yellow fluorescence signal in the cytoplasmic and plasma membrane regions of single cells (Fig. 2*C3* shows overlays of the green and red fluorescence signals).

TRPC1 transcripts are expressed by NSCs

We used PCR to detect the expression of *TRPC1* mRNA as well as those of six other *TRPCs* in dissociates of the telencephalon and in freshly sorted NSCs (Fig. 2*D*). *TRPC1–6* transcripts were all present in dissociates of the E13 telencephalon, although *TRPC4* mRNA was barely detectable. In contrast, *TRPC7* was not detectable in dissociates of the E13 telencephalon, whereas a very faint band was present in the freshly sorted NSC population. *TRPC1–4* and *TRPC6* mRNAs were all present in the NSC population. Thus, *TRPC4* seemed to be more enriched in the NSC fraction compared with that detected in the E13 telencephalic dissociate. Interestingly, *TRPC5* transcripts were present in the E13 telencephalic dissociate but not in the NSC population. The *TRPC5* band was instead found in the FACS-sorted early neuronal progenitor (ENP) population (data not shown). Thus, *TRPC1* mRNA is well expressed in NSCs along with four other *TRPCs*.

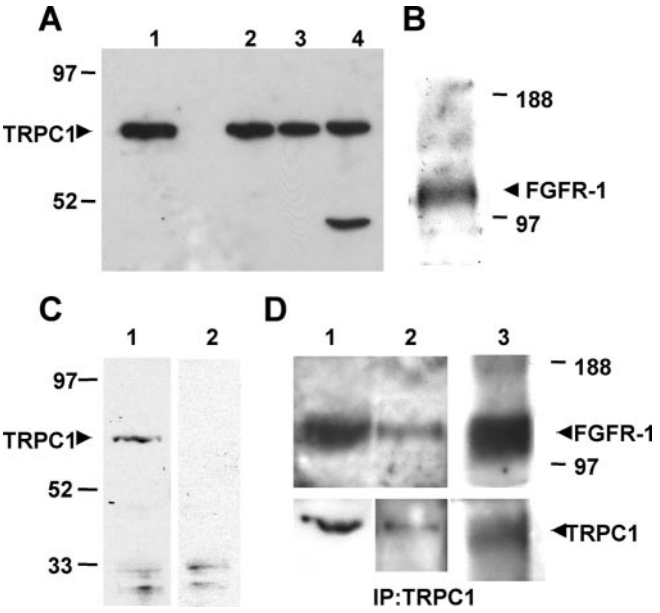

Figure 3. TRPC1 and FGFR-1 coimmunoprecipitate in membranes prepared from the E13 rat telencephalon. ***A***, ***B***, Membrane fractions obtained from the E13 rat telencephalon were probed on Western blots with anti-TRPC1-specific (***A***) and anti-FGFR-1-specific (***B***) antibodies. ***A***, Lanes 1–3 were loaded with different amounts of proteins (lane 1, 75 μg; lane 2, 50 μg; lane 3, 25 μg). HSG membrane fractions were used as a positive control (lane 4). Bands at the expected molecular weight (~92 kDa) are evident in all lanes. ***C***, Reactivity to anti-TRPC1 was detected in the microsomal fraction obtained from the E13 telencephalon (arrowhead; lane 1). Reactivity was blocked by preincubation of antibody with peptide (lane 2). ***D***, Immunoprecipitation of TRPC1 and FGFR-1 in the microsomal fraction. Detections of TRPC1 and FGFR-1 in the total lysate (lane 1), the solubilized fraction (lane 2), and in immunoprecipitates (lane 3) using the anti-TRPC1 antibody (Western blots using either anti-FGFR-1 or anti-TRPC1 antibodies) are shown. TRPC1 and FGFR-1 proteins are indicated by arrowheads.

TRPC1 and FGFR-1 coimmunoprecipitate in telencephalic membranes

Predominant coexpression of TRPC1 and FGFR-1 among proliferating NSCs led us to investigate possible interactions between them. A band of ~92 kDa corresponding to TRPC1 protein was detected in Western blots of telencephalic plasma membranes (Fig. 3*A*, lanes 1–3). HSG cells, which are known to express TRPC1, were used as a positive control (Fig. 3*A*, lane 4). The lower band (~52 kDa) that was detected in the crude membrane fraction of HSG cells has been described previously (Wang et al., 1999; Liu et al., 2000). Interestingly, this band was not detected in crude membranes prepared from the E13 rat telencephalon. FGFR-1 was also detected in the same membrane fraction as an ~120 kDa band, which represents the nonglycosylated form of the receptor, in accordance with the literature (Reilly et al., 2000; Kilkenny et al., 2003). Figure 3*C* shows the specificity of the anti-TRPC1 antibody. Detection of TRPC1 (Fig. 3*C*, lane 1) was completely blocked by incubation of anti-TRPC1 with the antigenic peptide (Fig. 3*C*, lane 2). To determine whether TRPC1 and FGFR-1 associate *in vivo*, we examined whether FGFR-1 coimmunoprecipitated with TRPC1 by using the TRPC1 antibody (Fig. 3*D*). Both proteins were detected in the total lysate and the solubilized fraction of the crude microsomal fraction (Fig. 3*D*, lanes 1, 2). FGFR-1 was highly enriched in the immunoprecipitate as well as TRPC1 (Fig. 3*D*, lane 3). Taken together, these data demonstrate that both TRPC1 and FGFR-1 are present in telencephalic membranes and can be immunoprecipitated as a complex, indicating that they are tightly associated with each other.

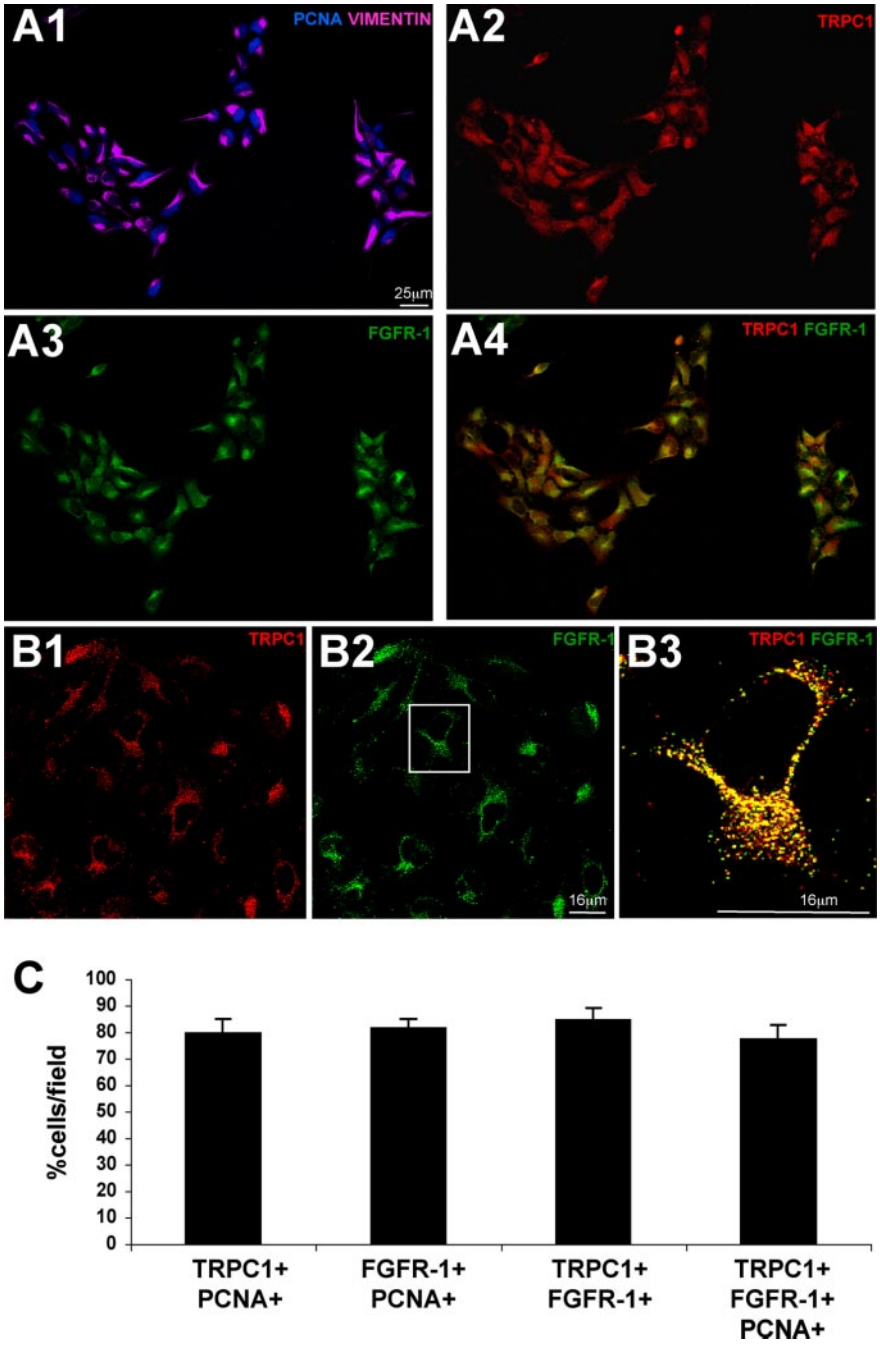

Figure 4. NSC-derived progeny coexpress TRPC1 and FGFR-1, which colocalize in the plasma membrane. NSCs were expanded for 7 d under self-renewing conditions (Neurobasal/B27 supplemented with 10 ng/ml bFGF), then their progeny were fixed and stained for TRPC1 and FGFR-1 in conjunction with PCNA and vimentin to reveal their proliferative (PCNA $^+$) and undifferentiated (vimentin $^+$) state. ***A1***, The merged image of PCNA and vimentin immunostaining demonstrates the proliferative and undifferentiated state of the NSC-derived progeny. ***A2***, ***A3***, Epifluorescence images of a representative field show that the great majority of the NSC-derived progeny express TRPC1 (***A2***) and FGFR-1 (***A3***). ***A4***, The merged image of both fluorescence signals reveals extensive colocalization of TRPC1 and FGFR-1. ***B1***, ***B2***, Confocal images show cellular localizations of TRPC1 (***B1***) and FGFR-1 (***B2***). ***B3***, Enlargement of the boxed field in ***B2*** reveals widespread membrane colocalization of TRPC1 and FGFR-1 immunoreactions. ***C***, Bar plot summarizes the quantitative analysis of 10 different fields. TRPC1 and FGFR-1 are coexpressed with PCNA and with each other in the majority of the NSC-derived progeny (75– 80%). Color-coded epitopes are identified in each panel.

TRPC1 and FGFR-1 colocalize in proliferating NSC-derived progeny *in vitro*

We used immunophenotyping and flow cytometry to isolate NSCs by negative selection (Maric et al., 2003) to study the role of TRPC1 channels in NSC proliferation and self-renewal without differentiation, which can be sustained in defined serum-free medium containing bFGF. After 7 d in culture, NSC-derived progeny remained morphologically immature, resembling the initial NSC founders. Multi-epitope immunostaining revealed that the majority of the progeny were actively proliferating (91% PCNA $^+$), and virtually all were immature precursors (99% vimentin $^+$) (Fig. 4*A1*) devoid of differentiating epitopes (data not shown), confirming previous results (Maric et al., 2003). The great majority (84%) of proliferating progeny coexpressed TRPC1 and FGFR-1 (Figs. 4*A2–A4*, 5*C*), whereas few were either single-positive TRPC1 $^+$ (9%) or FGFR-1 $^+$ (6%) and only ~1% were TRPC1 $^-$FGFR-1 $^-$. Most PCNA $^+$ cells were TRPC1 $^+$ (79%) or FGFR-1 $^+$ (81%) (Fig. 4*C*). These widespread coexpressions resulted in the majority of immature NSC-derived progeny (77%) being TRPC1 $^+$ FGFR-1 $^+$ PCNA $^+$ (Fig. 4*C*). Therefore, TRPC1 and FGFR-1 were coexpressed in most NSC-derived progeny proliferating *in vitro* in the presence of bFGF.

Confocal microscopy was used to resolve the localization of TRPC1 and FGFR1 in single cells. TRPC1 and FGFR-1 signals were localized in the plasma membrane and subplasma membrane regions, as well as in the cytoplasm of cells (Fig. 4*B1*,*B2*). Subcellular colocalization of TRPC1 and FGFR-1 in individual cells was reflected by the presence of intricate yellow fluorescence signals corresponding to the merge of the individual green and red immunoreactivities (Fig. 4*B3*).

Collectively, the data indicate that, similar to NSCs profiled *ex vivo*, TRPC1 and FGFR-1 are coexpressed in the majority of the actively proliferating NSC-derived progeny, where they are colocalized in both cytoplasmic and membrane regions.

Antisense/TRPC1 treatment attenuates TRPC1 expression but not other TRPCs in proliferating NSC-derived progeny

NSCs were plated at clonal density and incubated with either antisense/TRPC1 ODN or missense ODNs over a 7 d period. FITC-labeled ODNs were taken up by the majority of proliferating progeny as reflected by the green fluorescence signals associated with many of the cells (Fig. 5*A2*). RT-PCR showed that treatment with antisense ODN markedly reduced the presence of *TRPC1* mRNA, whereas treatment with missense did not (Fig. 5*B*). Treatment with the antisense/TRPC1 ODN did not affect the transcript abundance of a housekeeping gene (*L-19*), demonstrating that the lack of *TRPC1* transcripts was not attributable to improper amplification (Fig. 5*B*). Quantitation of TRPC1 immunofluorescence signal intensities in fields of NSC-derived progeny revealed that antisense/

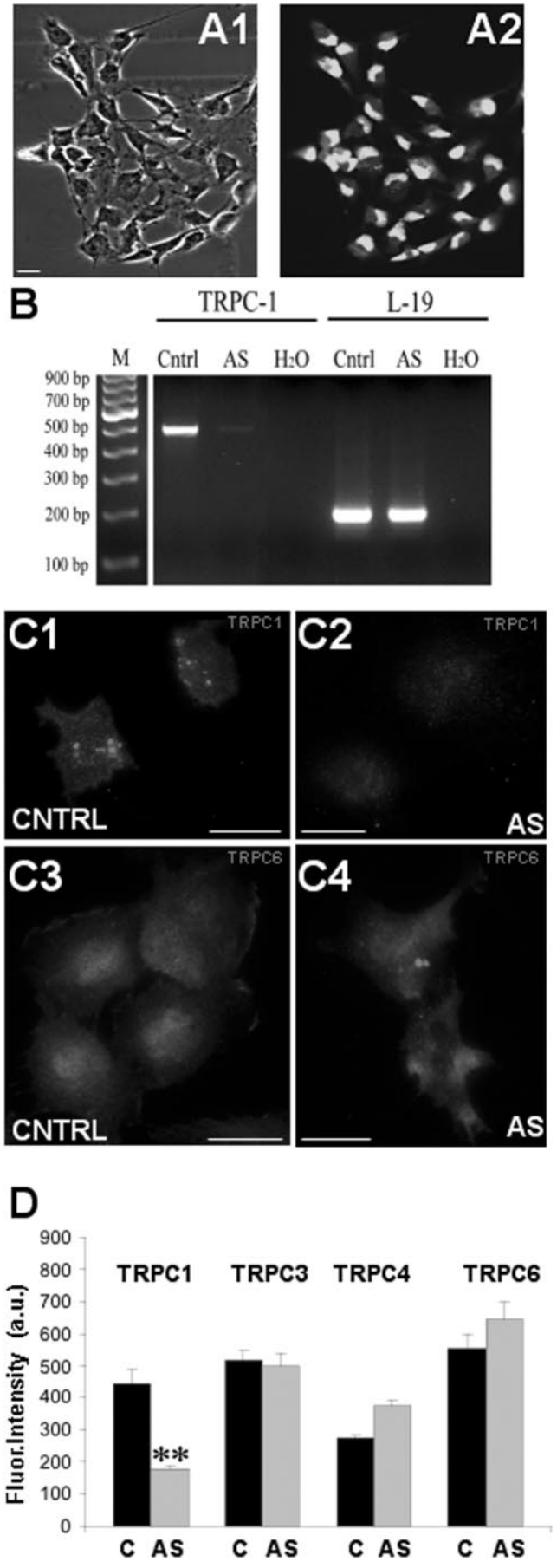

TRPC1 significantly reduced the intensity of the fluorescence signals compared with missense treatment (Fig. 5*C1*,*C2*,*D*). To test whether antisense/TRPC1 treatment was specific for TRPC1 protein expression, we analyzed the effect of antisense/TRPC1 ODN on other TRPC expressions. As an example, Figure 5, *C3* and *C4*, shows that TRPC6 expression was not affected by antisense/TRPC1 treatment compared with missense-treated cells. Quantitation of immunofluorescence signal intensities revealed that TRPC3, TRPC4, or TRPC6 was not affected by antisense/TRPC1 treatment (Fig. 5*D*). In addition, RT-PCR data show that *TRPC2* levels did not change in antisense/TRPC1-treated cells compared with missense-treated cells (data not shown).

These results establish that antisense/TRPC1 effectively knocks down TRPC1 transcripts as well as proteins without affecting the expressions of other TRPCs expressed by NSC-derived progeny.

Antisense/TRPC1 treatment attenuates NSC proliferation

To test whether antisense treatment affected proliferation, NSCs were plated at clonal density and allowed to expand under self-renewing conditions in defined medium with bFGF for 7 d. Two concentrations of antisense/TRPC1 ODNs were used (2 and 5 μM). Both concentrations significantly reduced the total number of cells per clone compared with missense treatments and decreased the percentage of proliferating ($PCNA^+$) cells per clone (Fig. 6*A*,*B*). There was not a significant difference ($p > 0.05\%$) in the percentage of total cell death (because of either pyknosis or apoptosis) between the antisense/TRPC1-treated cells (4.9 ± 1.1 and $5.2 \pm 1.5\%$, respectively, at 2 and 5 μM) and missense-treated cells (3.1 ± 0.7 and $2.5 \pm 0.6\%$, respectively, at 2 and 5 μM), indicating that cell death did not account for the decrease in clone size. The results indicate that knock-down of TRPC1 channel proteins attenuates NSC proliferation without causing significant cell death. Furthermore, the knock-down of TRPC1 proteins did not induce NSCs to differentiate.

Because TRPC1 channel proteins comprise voltage-independent Ca^{2+} channels, we compared the effects of an inorganic (Gd^{3+}) and an organic (SKF96365) (Beech et al., 2003) antagonist of Ca^{2+} entry, which are commonly used to block voltage-independent Ca^{2+} channels, and an antagonist at L-type voltage-dependent Ca^{2+} entry (nitrendipine) on NSC proliferation. Both Gd^{3+} (1 μM) and SKF96365 (1 μM) significantly reduced clone size and the percentage of proliferative cells (Fig. 6*C*–*F*). In contrast, nitrendipine did not affect either of these parameters (Fig. 6*C*,*E*). Furthermore, in the presence of Gd^{3+} or SKF96365, the percentages of total cell death ($10.5 \pm 2\%$ for Gd^{3+} and $8.9 \pm 1.5\%$ for SKF96365) were not

←

Figure 5. TRPC1 antisense treatment of NSC-derived progeny decreases TRPC1 transcripts and protein expression. Phase contrast (***A1***) and epifluorescence (***A2***) images of a representative field of NSC-derived progeny show that FITC-labeled ODNs are taken up by virtually all progeny after 7 d in culture. ***B***, Analysis of TRPC1 mRNA levels reveals clear effects of NSCs treated with control (Cntrl) and TRPC1 antisense (AS) ODNs (5 μM). Equal amounts of RNA were reversed transcribed to generate cDNA. The cDNA was subjected to TRPC1-specific PCR amplification (500 bp product) using paired primers. cDNA from all samples was also subjected to *L-19*-specific PCR amplification (195 bp product). The left lane shows a ladder of molecular weight markers (M). Note the dramatic reduction of TRPC1 mRNA in NSC-derived progeny treated for 7 d with antisense ODNs compared with treatment with control ODNs. ***C1–C4***, Representative images of antisense/TRPC1-treated cells (AS) and missense-treated cells (CNTRL) stained for TRPC1 or TRPC6. The data show a clear difference in TRPC1 expression between CNTRL and AS, whereas no difference is evident in TRPC6 expression. ***D***, Fluorescence intensities of TRPC1, TRPC3, TRPC4, and TRPC6 protein expressions in NSC-derived progeny shows a significant (**$p < 0.005$) reduction in progeny treated with 5 μM antisense TRPC1 (AS) compared with treatment with equimolar control ODNs (C) for TRPC1 but not for the other TRPCs studied. Scale bars, 10 μm

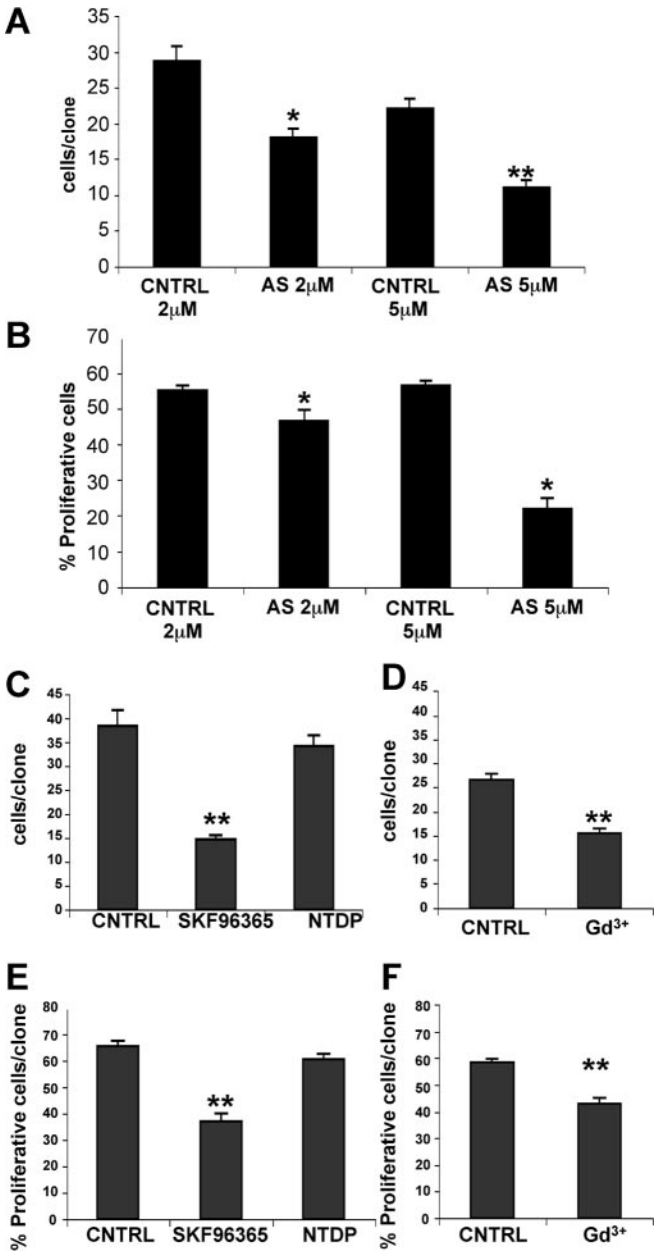

Figure 6. NSC proliferation is inhibited by antisense/TRPC1 and antagonists of voltage-independent Ca^{2+} entry. NSCs were plated at clonal density and cultured for 7 d under different conditions. After multi-epitope staining with lineage-specific markers, 10 clones from three independent experiments were quantified to reveal the total cell number per clone (***A***, ***C***, ***D***) and the percentage of proliferative cells per clone (***B***, ***E***, ***F***). ***A***, ***B***, NSC progeny were grown for 7 d in the presence of antisense/TRPC1 and control ODNs to test for a role of TRPC1 in bFGF-mediated NSC proliferation. Both 2 and 5 μM antisense TRPC1 (AS) induce a significant reduction in the number of cells per clone as well as in the percentage of proliferative cells compared with treatment with control ODNs (CNTRL). ***C–F***, NSC progeny were grown for 7 d under either self-renewing conditions (CNTRL) or in the presence of organic (SKF96365; 1 μM) or inorganic (Gd^{3+}; 1 μM) antagonists of voltage-independent Ca^{2+} channels or an organic blocker of L-type Ca^{2+} channels [nitrendipine (NTDP); 10 μM]. Both SKF69365 and Gd^{3+} significantly reduce clone size and the percentage of proliferative cells in clones. Nitrendipine is ineffective (*$p < 0.01$; **$p < 0.005$).

significantly different ($p > 0.01$) compared with controls (3.8 ± 1.9 and 5.8 ± 0.7%, respectively, for Gd^{3+} and SKF96365). These results indicate that the effects of the drugs were not simply attributable to toxic actions and that cell death did not account for the decrease in clone size. Thus, different blockers of receptor-operated Ca^{2+} entry channels mimic the effect of antisense treatment, whereas antagonism of a major voltage-dependent pathway does not. These results are consistent with a role for voltage-independent Ca^{2+} channels including TRPC1 in sustaining NSC proliferation.

Antisense/TRPC1 treatment attenuates bFGF-induced Ca_i^{2+} responses

NSC-derived progeny proliferating in bFGF respond to bFGF with elevations in $[Ca^{2+}]_i$ containing an initial peak and a later sustained phase (Maric et al., 2003). To test whether antisense/TRPC1 treatment affected regulation of $[Ca^{2+}]_i$ by bFGF, we performed imaging experiments in cells treated with missense or antisense/TRPC1 ODN for 7 d. Peak and sustained Ca_i^{2+} responses to bFGF were readily detected in proliferating NSC-derived progeny treated with missense (Fig. 7*A1*). In contrast, there was a modest decrease in the peak amplitude of the bFGF-induced Ca_i^{2+} signal and a dramatic decrease in the amplitude of the sustained phase after treatment with antisense/TRPC1 ODN (Fig. 7*A2*). Statistical analysis of the results showed that the reduction in peak amplitude was not significant (Fig. 7*B1*), whereas the decline in the sustained phase was significant (Fig. 7*B2*).

Additionally, we compared bFGF-induced Ca_i^{2+} signals in Ca^{2+}-free medium to exclude Ca^{2+} entry. Transient Ca_i^{2+} responses to bFGF, reflecting Ca^{2+} release from intracellular stores, were virtually identical in cells treated with missense and antisense/TRPC1 ODNs (Fig. 7*C1–C3*). Thus, downregulation of TRPC1 mRNA and proteins did not affect bFGF/FGFR-1 signaling that triggers Ca^{2+} release. Rather, the external Ca^{2+}-dependent contribution to the response (i.e., Ca^{2+} entry) is attenuated. To show that Ca^{2+} entry can also be triggered independently of bFGF, we exposed cells treated with missense or antisense/TRPC1 ODN to the membrane-permeant analog of diacylglycerol (DAG), 1-oleoyl-2-acetyl-*sn*-glycerol (OAG), which is thought to activate Ca^{2+} entry via TRPC channels not composed of TRPC1 subunits (for review, see Clapham, 2003). OAG evoked Ca_i^{2+} responses that were not significantly different in amplitude and time course in missense- and antisense/TRPC1-treated cells (Fig. 7*D1–D3*). Together, these results demonstrate that antisense/TRPC1 treatment affects the Ca^{2+} entry components of the Ca_i^{2+} response to bFGF without apparently affecting Ca^{2+} release. The lack of effect of antisense treatment on OAG-induced Ca_i^{2+} responses suggests that other voltage-independent Ca^{2+} channels putatively containing DAG-sensitive TRPC channel proteins are not affected.

The effect of antisense/TRPC1 treatment on the biphasic peak-and-plateau Ca_i^{2+} response to bFGF in the absence of any effects on bFGF-evoked Ca_i^{2+} signals in Ca^{2+}-free medium, which involve Ca^{2+} release, led us to study agents known to block Ca^{2+} entry in other cell types. Both SKF96365 (Fig. 8*A2*) and Gd^{3+} (Fig. 8*A3*) simplified the peak-and-plateau Ca_i^{2+} response to bFGF (Fig. 8*A1*) into one dominated by only a transient phase. This would be expected if both agents blocked the Ca^{2+} entry component but not the Ca^{2+} release component. The Ca_i^{2+} transients illustrated in Figure 8, *A2* and *A3*, closely resemble those shown in Figure 7, *C1* and *C2*, which demonstrate bFGF-induced Ca_i^{2+} transients in the absence of extracellular Ca^{2+}. Not only was the sustained phase of the biphasic response to bFGF mostly eliminated by SKF96365 and Gd^{3+}, but the peak amplitudes of the Ca_i^{2+} responses were significantly reduced (Fig. 8*A4*). This shows that Ca^{2+} entry also contributes to the initial peak of the Ca_i^{2+} response to bFGF. A clear and partly reversible depression of the sustained phase was readily apparent with both Gd^{3+} (Fig. 8*B1*) and SKF96365 (data not shown). Both of these effects were significant (Fig. 8*B2*). Finally, nitrendipine did not significantly affect the peak-and-plateau Ca_i^{2+} response to bFGF (Fig.

8*C1*,*C2*), demonstrating that voltage-dependent Ca^{2+} channels are not involved.

Based on these data, we suggest that a significant part of the biphasic Ca_i^{2+} response to bFGF involves Ca^{2+} entry mediated by voltage-independent Ca^{2+} channels. Our data showing that antisense/TRPC1 treatment attenuates this Ca^{2+} entry are consistent with this suggestion and indicate that TRPC1 channels mediate, at least in part, the Ca^{2+} influx induced by bFGF/FGFR-1 signaling.

Antisense/TRPC1 treatment depresses bFGF-induced current responses and conductance changes

The presence of a Ca^{2+} entry component throughout the biphasic Ca^{2+} response to bFGF and its sensitivity to both antisense and pharmacological treatments led us to use patch-clamp techniques to measure the currents stimulated by bFGF. Proliferating NSC-derived progeny were washed in bFGF-free saline solution and then clamped in the whole-cell mode to record cation currents in response to brief applications of bFGF. Cells were held at 0 mV and subjected to voltage ramps from −90 to +90 mV every 4 s. The traces shown in Fig. 9, *A–C* and E, represent bFGF-stimulated inward currents that have been reconstructed from the current amplitudes at −80 mV obtained from current responses to the intermittently imposed 1 s voltage ramps. The latter were used to construct *I–V* curves (Fig. 9*D*,*F*). We have illustrated bFGF-induced currents stimulated at −80 mV because this membrane potential is in the range previously reported for intact neuroepithelial cells studied with a calibrated potentiometric dye strategy and flow cytometry (Maric et al., 1998b) and because the current responses were readily detectable at this potential. bFGF triggered inwardly directed currents in all of the cells recorded, consistent with there being a quite widespread distribution of bFGF-induced Ca^{2+} responses among these cells. Superfusion of either Gd^{3+} (Fig. 9*A*) ($n = 3$ cells) or SKF96365 (Fig. 9*B*) ($n = 3$ cells) completely inhibited the bFGF-induced inward currents, which returned to baseline levels in all cells tested. The results are consistent with bFGF activation of voltage-independent cation conductance. From previous studies of mechanisms regulating $[Ca^{2+}]_i$ in neuroepithelial cells at the beginning of neurogenesis, we found no evidence of voltage-dependent Ca^{2+} entry contributing to $[Ca^{2+}]_i$ at this stage of development (Maric et al., 2000a). In addition, nitrendipine did not affect the peak-and-sustained Ca_i^{2+} responses to bFGF (Fig. 8*C1*,*C2*). Perfusion of DVF medium during the bFGF-induced current response transiently increased the amplitude of the inwardly directed current (Fig. 9*C*), which then relaxed to baseline levels ($n = 4$ cells). The current relaxation in the cell illustrated began before exposure to the DVF solution,

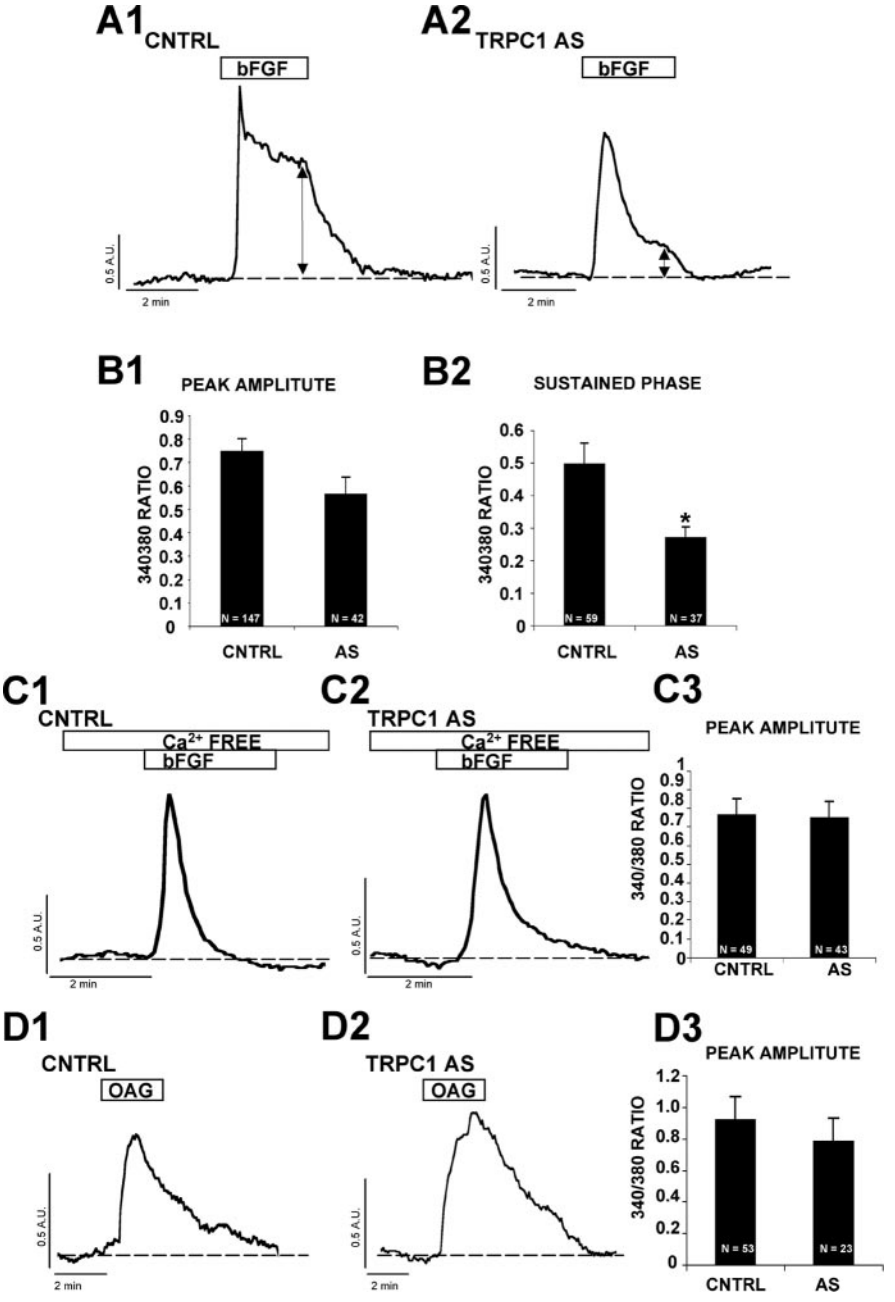

Figure 7. bFGF-mediated Ca^{2+} entry is inhibited by antisense/TRPC1 treatment. NSCs were cultured in the presence of antisense/TRPC1 and missense ODNs; after 7 d, the cells were loaded with fura-2 and then imaged to detect bFGF-induced Ca_i^{2+} signals. ***A***, Two representative traces show bFGF-mediated Ca_i^{2+} signals in cells treated with missense ODN (CNTRL) (***A1***) and TRPC1 antisense (AS) (***A2***). ***B1***, ***B2***, The amplitudes of the initial transient peak and the sustained phase were quantified, and the results have been summarized in bar plots. There is no statistically significant difference in the amplitudes of the initial transient peak (***B1***), whereas there is a significant reduction in the sustained phase ($^*p < 0.005$) after antisense/TRPC1 treatment compared with control ODN. ***C1–C3***, bFGF (10 ng/ml) triggers a self-limiting Ca_i^{2+} transient in Ca^{2+}-free medium, reflecting exhaustive Ca^{2+} release from intracellular stores, which is virtually identical in cells treated with either missense ODN (***C1***) or TRPC1 antisense (***C2***). ***C3***, Quantitative summary of the results in bar plot format. ***D1***, ***D2***, A concentration of 25 μM OAG applied to cells treated with missense ODN (***D1***) or TRPC1 antisense (***D2***) evokes similar Ca_i^{2+} responses. ***D3***, Bar plot of the quantified peak amplitudes of the OAG-induced Ca_i^{2+} signals show no significant difference between OAG-induced amplitudes evoked in cells treated with TRPC1 antisense compared with control ODNs. In ***A1***, ***A2***, ***C1***, ***C2***, ***D1***, ***D2***, the experimental logs are shown above the Ca^{2+} traces, and the dashed lines at the bottom indicate baselines. Double-ended arrows in ***A1*** and ***A2*** indicate the sustained phase amplitude. The numbers inside the bars indicate the total number of cells analyzed.

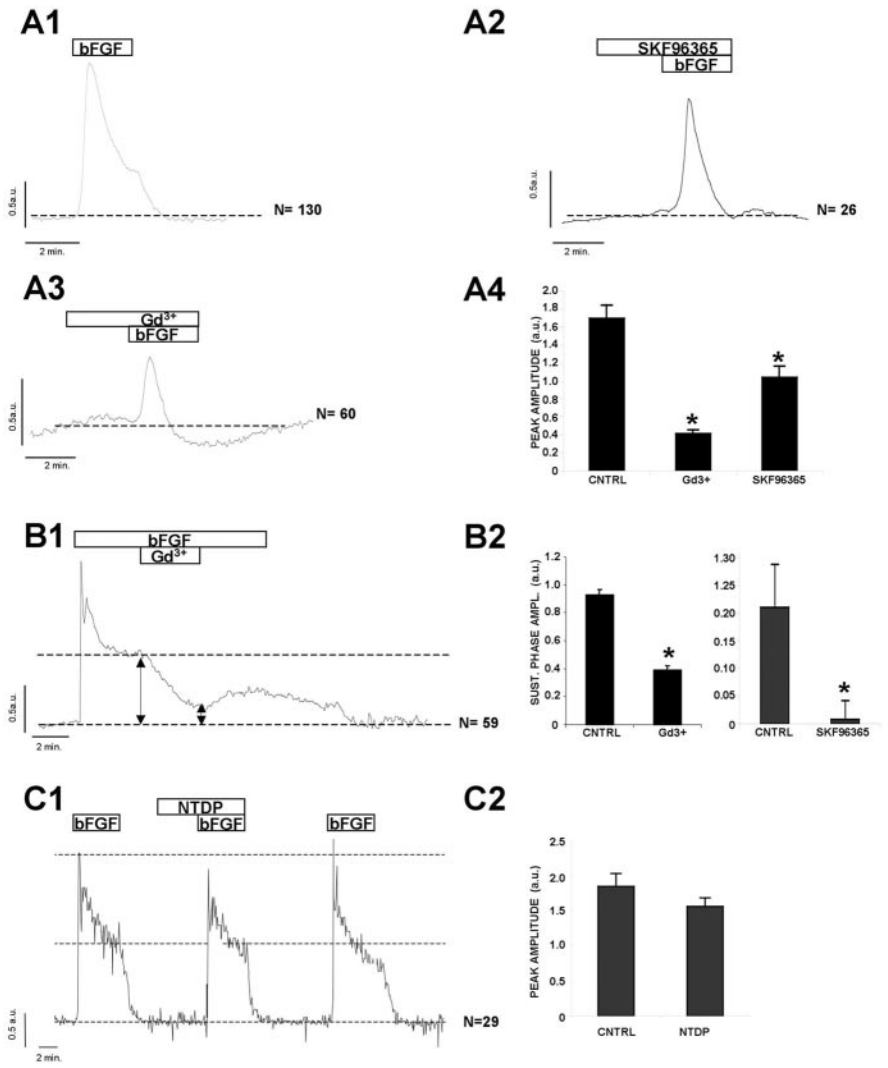

Figure 8. bFGF-mediated Ca^{2+} entry is blocked by antagonists of voltage-independent Ca^{2+} channels. NSC-derived progeny were imaged using methods outlined in the Figure 7 legend. Experimental conditions are logged above the corresponding Ca_i^{2+} traces (***A1–A3***, ***B1***, ***C1***), which are representative of the results (summarized in ***A4***, ***B2***, and ***C2***). The numbers (N) at the ends of the traces indicate the total number of cells analyzed. The dashed lines depict the baselines of individual cells and in ***B1*** and ***C1***, the trajectory of the sustained phase of the Ca_i^{2+} response during prolonged exposure to bFGF. ***A1***, bFGF (10 ng/ml) triggers Ca_i^{2+} signals composed of a transient and a sustained phase. ***A2***, ***A3***, A significant decrease in the initial peak amplitude of the Ca^{2+} signal and elimination of the sustained phase is observed in the presence of 1 μM SKF69365 or 1 μM Gd^{3+} compared with the control. ***A4***, Bar plot summarizes the significant decreases in peak amplitudes compared with control (CNTRL). ***B1***, Prolonged exposure to 10 ng/ml bFGF sustains Ca_i^{2+} levels, which are blocked by 1 μM Gd^{3+} in a partially reversible manner. ***B2***, Bar plot summarizes the effects of Gd^{3+} and SKF69365 on the sustained phase (*$p < 0.005$). Double-ended arrows in ***B1*** indicate the sustained phase amplitude before and during the applications of Gd^{3+}. ***C1***, ***C2***, Nitrendipine (NTDP; 10 μM) has no significant effect on the bFGF-induced Ca_i^{2+} response. ***C2***, Bar plot summarizes the results and shows no significant difference.

which accelerated the decline. The transient increase in current is consistent with the nonspecific cation selectivity of voltage-independent channels. *I–V* curves under control and perfusion with DVF conditions show that, in the latter, the reversal potential of the *I–V* curve shifts slightly in the negative direction but still remains positive (approximately +5mV). In addition, the slope of the *I–V* curve increased, reflecting a transient increase in the membrane conductance in DVF saline in response to bFGF. These results are consistent with the well known unblocking effect of DVF solutions on voltage-independent channels with a relatively broad selectivity for cations. In the absence of divalent cations, ambient monovalent cations (Na^+ and K^+) are conducted more easily, thus generating more inward current at negative potentials and leading to a reversal potential nearer to 0 mV. These results led us to test the effect of exposure to a saline in which all the extracellular Na^+ and Ca^{2+} ions were replaced by NMDG. Switching from normal to NMDG saline rapidly eliminated the bFGF-induced current response (Fig. 9*E*) and associated conductance (Fig. 9*F*) in a completely reversible manner ($n = 3$ cells). Thus, bFGF activates inward currents at negative potentials, which reverse polarity at approximately +15 mV and are completely blocked by both Gd^{3+} and SKF96365, and by either exposure to a DVF solution or to an Na^+- and Ca^{2+}-free saline. These characteristics are consistent with the activation of bFGF of voltage-independent cation channels with relatively little selectivity over monovalent and divalent cations.

In missense-treated cells, the current activated by bFGF increased, reached a maximum in ~40–60 s and remained sustained for ~40–60 s after bFGF was washed out, then gradually declined (Fig. 10*A1*), similar to responses recorded under control conditions (Fig. 9). In antisense/TRPC1-treated cells, the current response was lower in amplitude (1083 ± 27 pA in six missense-treated cells, 358 ± 104 pA in eight antisense/TRPC1-treated cells) and declined quickly after removal of bFGF (Fig. 10*A1*). There was a significant decrease in the bFGF-activated current density measured at the peak of the current response in antisense/TRPC1-treated cells compared with control cells (Fig. 10*A2*). The individual voltage ramps obtained at the peak of the bFGF-evoked responses showed relatively linear *I–V* relationships with a reversal potential of approximately +15 mV (Fig. 10*B*), similar to those recorded in untreated cells (Fig. 9). In antisense/TRPC1-treated cells, neither the reversal potential nor the character of the *I–V* curve was altered (Fig. 10*B*). These results indicate that the decrease in the peak amplitude of the bFGF-evoked inward current was not attributable to a change in the driving force acting on the activated channels but rather to a decrease in their conductance.

Discussion

Salient findings

FACS analyses reveal that TRPC1 is expressed by the majority of proliferating NSCs, which also express FGFR-1, along with TRPC2, TRPC3, TRPC4, and TRPC6. As NSCs differentiate, TRPC1 expression progressively decreases, whereas FGFR-1, TRPC2, TRPC3, TRPC4, and TRPC6 remain relatively constant. TRPC1 and FGFR-1 coimmunoprecipitate from solubilized telencephalic membranes and colocalize in the membrane and cytoplasm of NSCs and their progeny. Antisense/TRPC1 treatment reduces TRPC1 transcript and protein expression in proliferating NSC progeny, without affect-

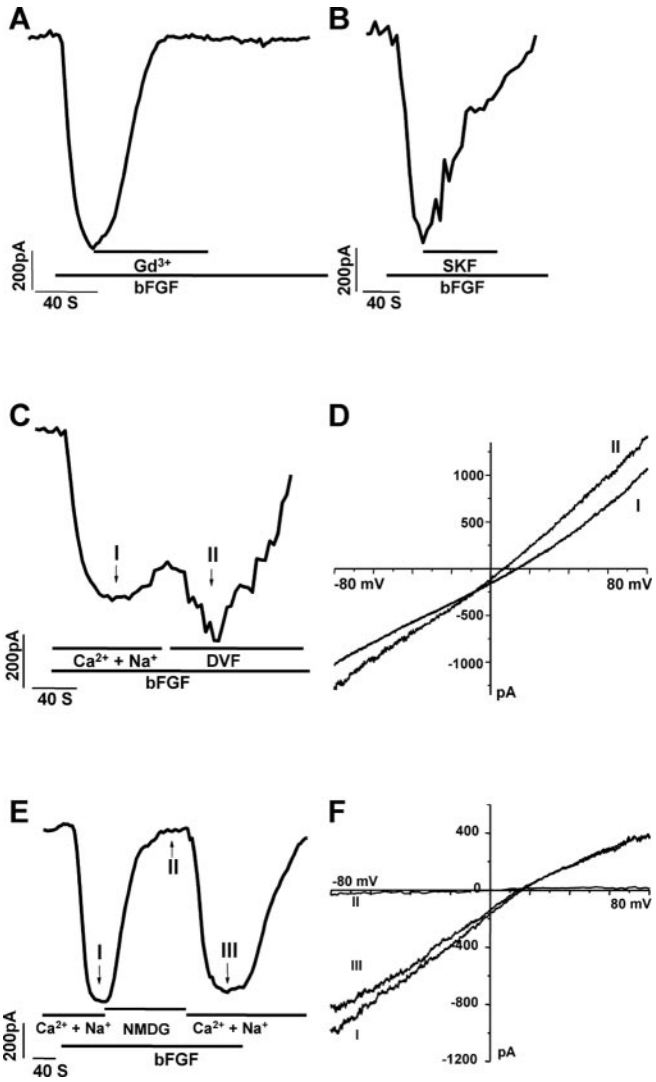

Figure 9. Pharmacological block of bFGF-induced currents and their sensitivity to DVF and Na^+/Ca^{2+}-free saline. NSC-derived progeny were expanded in medium with 10 ng/ml bFGF and then rinsed in bFGF-free saline before patch-clamp recordings were performed in the whole-cell mode. The cells were clamped at 0 mV, and 1 s voltage ramps over the −90 to +90 mV range were applied every 4 s. Current traces at −80 mV before and during perfusion of bFGF in different salines were reconstructed from the protocol. ***A***, Perfusion of 10 ng/ml bFGF triggers an inwardly directed current that peaks in ~60 s. Coapplication of 1 μM Gd^{3+} rapidly and completely reduces the current response, which does not recover after stopping the Gd^{3+} perfusion. ***B***, Coapplication of 1 μM SKF96365 (SKF) rapidly blocks the bFGF-induced current response, which does not recover during the recording period. ***C***, bFGF induces an inward current (I), which transiently increases in amplitude (II) when DVF saline is perfused instead of normal saline containing Ca^{2+} and Mg^{2+} before relaxing to baseline. ***D***, *I–V* plot of bFGF-induced currents in normal saline containing Ca^{2+} and Mg^{2+} (I) and in DVF (II) demonstrate relatively linear plots with similar reversal potentials (+15 mV in normal saline, +5 mV in DVF). The slope of the *I–V* plot increases in DVF, reflecting an increase in conductance. ***E***, Perfusion of NMDG solution, which does not contain either Na^+ or Ca^{2+}, rapidly and completely blocks the bFGF-induced current response in a reversible manner. ***F***, The *I–V* plot demonstrates the reversibility in the underlying bFGF-induced conductance. The traces shown are representative of three cells in Gd^{3+} and SKF96365 experiments, four cells in the DVF experiments, and three cells in the NMDG experiments.

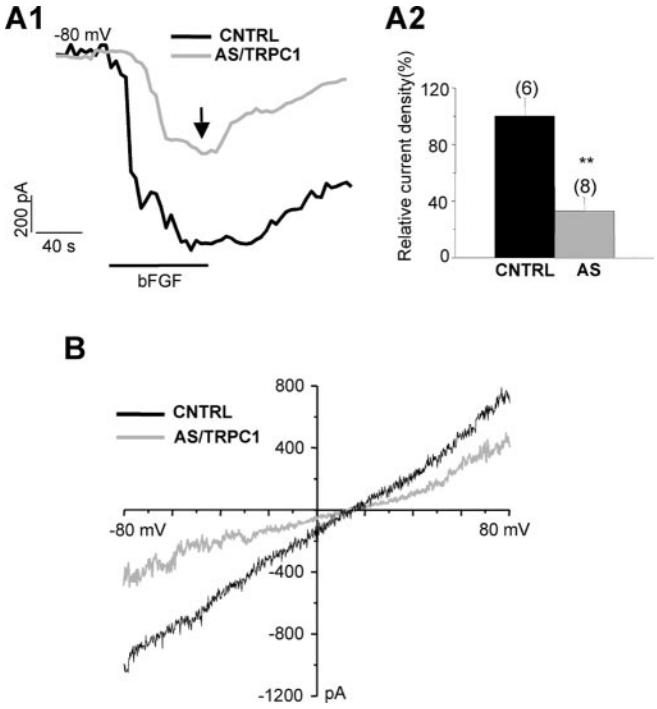

Figure 10. Antisense/TRPC1 depresses bFGF-induced currents in NSC-derived progeny. NSC-derived progeny proliferating in medium with bFGF were rinsed with bFGF-free saline before recordings from the cells in whole-cell patch-clamp mode. ***A1***, Inwardly directed cation current responses are detected after perfusion with medium containing 10 ng/ml bFGF. The current is reduced in cells treated with antisense/TRPC1 (AS/TRPC1; gray trace) compared with those treated with missense ODNs (CNTRL; black trace). ***A2***, bFGF-activated current densities are significantly reduced in antisense/TRPC1-treated cells (AS; gray bar) compared with those treated with missense ODNs (CNTRL; black bar). Current densities of the control group are normalized to 100%. (**$p < 0.01$). The number of cells measured in each group is noted in parentheses above each bar. ***B***, *I–V* relationships at the peak of the bFGF-induced currents are relatively linear in both antisense- and missense-treated cells with current reversing polarity at approximately +15 mV, indicating that the decrease in bFGF-evoked current amplitude reflects a reduction in membrane conductance.

ing other TRPC expressions, and decreases clone size and the percentage of proliferating cells, without significantly affecting cell death. Similar effects occur when NSC progeny are treated with antagonists of voltage-independent Ca^{2+} channels. Antisense/TRPC1 treatment and antagonists of voltage-independent Ca^{2+} channels reduce the Ca^{2+} entry component contributions to the bFGF-activated peak-and-plateau Ca_i^{2+} response and attenuate or eliminate current responses and associated conductance changes. Together, the results demonstrate a role for TRPC1-mediated Ca^{2+} entry during self-renewal of proliferating NSCs sustained by bFGF/FGFR-1 signaling.

TRPC1 and FGFR-1 are coexpressed in the embryonic rat telencephalon

TRPC1-immunoreactive cells were mostly located adjacent to the LV in the telencephalon, although some immunopositive cells were also found within the neuroepithelium. Quantitative FACS analyses demonstrated that most of the NSCs expressed TRPC1 and FGFR-1 and were actively proliferating. Furthermore, the relatively close correspondence between the percentages of $PCNA^+$ and $TRPC1^+$ cells among the five progenitor populations suggest that TRPC1 expression is closely linked to proliferation during the initial stages of NSC differentiation. The coexpression of TRPC1 and FGFR-1 in $PCNA^+$ NSCs *in vivo* and the ability of bFGF to sustain self-renewal of NSCs *in vitro* strongly suggest that maintenance of the NSC pool *in vivo* includes a pathway involving bFGF, FGFR-1, and TRPC1. There is evidence *in vivo* for bFGF and FGFR-1 playing critical roles in neurogenesis of the cortex. bFGF knock-out mice are missing about one-half of glutamatergic pyramidal neurons in the anterior cortex (Vac-

carino et al., 1999a; Korada et al., 2002). This is attributable to a corresponding loss in neuroepithelial cells composing the dorsal telencephalon in early neurogenesis (Vaccarino et al., 1999a; Raballo et al., 2000). Recently, a transgenic mouse strain conditionally overexpressing a tyrosine kinase domain-deficient FGFR-1 gene construct has generated the same phenotype (Shin et al., 2004). Thus, bFGF activation of FGFR-1 is critical for generating and maintaining a population of precursors, the progeny of which differentiate into pyramidal neurons. No data have been reported to demonstrate a role for TRPC1 in neurogenesis.

In our study, TRPC1 and FGFR-1 coimmunoprecipitated from telencephalic membranes, indicating that they interact either directly or indirectly in a complex. An interaction between tyrosine kinase receptors and TRPC channels has previously been reported in pontine neurons in which TRPC3 has been proposed to be activated through a pathway that is initiated by brain-derived nerve growth factor activation of the tyrosine kinase receptor TrkB (Li et al., 1999). Furthermore, there are different experimental observations supporting the hypothesis that TRPC1 functions within a signalplex in non-neuronal (Lockwich et al., 2000; Rosado and Sage, 2001; Singh et al., 2001, 2002) and neuronal cells, including the adaptor protein Homer, which facilitates a physical association between TRPC1 and IP_3 receptor that is required for the channel to respond to signals (Kim et al., 2003; Yuan et al., 2003).

TRPC1-mediated Ca^{2+} influx is important in NSC proliferation

An important finding was that TRPC1 is involved in NSC self-renewal *in vitro* and in bFGF-mediated Ca^{2+} influx. Similar to NSCs profiled *ex vivo* with flow cytometry, 75–80% of self-renewing NSC-derived progeny were $PCNA^+$ $TRPC1^+$ $FGFR\text{-}1^+$. *Ipso facto*, bFGF/FGFR-1 signaling via TRPC1 could serve to sustain symmetrical divisions of self-renewing NSCs *in vivo*.

Antisense/TRPC1 treatment, which decreased TRPC1 transcript as well as protein levels in NSC-derived progeny, also reduced both the clone size and percentage of proliferating cells. These effects indicate that TRPC1 channels are associated with NSC proliferation. Importantly, antisense/TRPC1 treatment did not induce significant cell death. Similar effects on clone size and the percentage of proliferative cells were obtained by including pharmacological antagonists of agonist-stimulated Ca^{2+} entry channels in the culture medium, whereas a blocker of L-type Ca^{2+} channels was ineffective. Together, these results support the conclusion that Ca^{2+} entry via TRPC1 channels stimulated by bFGF/FGFR-1 signaling sustains NSC proliferation *in vitro*.

Many developmental studies on Ca^{2+} signaling during organogenesis have established Ca^{2+} as a ubiquitous second messenger, the regulation of which in cells is critical to each phase of development beginning with proliferation (for review, see Webb and Miller, 2003). A variety of mitogenic agonists are known to stimulate the growth of different cell phenotypes by increasing $[Ca^{2+}]_i$ levels (Kao et al., 1990; Chao et al., 1992; Pitt et al., 1994). In this regard, human pulmonary arterial smooth muscle cell proliferation stimulated by serum and growth factors is attenuated by chelating extracellular Ca^{2+} and depleting intracellular stores (Golovina et al., 2001). Although smooth muscle cells express functional voltage-dependent L-type Ca^{2+} channels, the constant Ca^{2+} influx, as well as that after store–depletion, involves voltage-independent TRP-type Ca^{2+} channels. TRPC1 expression is upregulated during human smooth muscle cell proliferation, and inhibition of its expression attenuates proliferation as well as store–depletion-induced Ca^{2+} influx (Sweeny et al., 2002a). Entirely similar results have also been obtained in a study on proliferating rat bronchial smooth muscle cells in terms of establishing a critical role for TRPC1 in sustaining both proliferation and elevated $[Ca^{2+}]_i$ required for proliferation (Sweeney et al., 2002b). Thus, TRPC1 cation channels activated by growth factors and serum mediate the Ca^{2+} entry necessary to sustain the elevated $[Ca^{2+}]_i$ levels associated with smooth muscle cell proliferation.

Similar to smooth muscle cells, embryonic rat cortical neuroepithelial cells require physiological Ca^{2+} levels for growth factor-mediated proliferation (Ma et al., 2000). Flow cytometric analyses of proliferating neuroepithelial cells profiled *ex vivo* and imaging of cells *in vitro* have revealed significant contributions of Ca^{2+} entry to baseline Ca_i^{2+} levels among proliferating undifferentiated precursors (Maric et al., 2000b). This study also demonstrated that voltage-dependent mechanisms are not involved in constitutive Ca^{2+} entry expressed by these cells.

Here, we show that the bFGF-mediated Ca_i^{2+} response was attenuated by treatment with antisense/TRPC1 and by blockers of voltage-independent Ca^{2+} channels. The treatment affected the sustained phase significantly. The effects of antisense/TRPC1 treatment clearly target TRPC1 channels involved in Ca^{2+} entry, because there was no effect of antisense treatment on bFGF-evoked release of Ca^{2+} from intracellular stores in Ca^{2+}-free medium. The role of TRPC1 in bFGF-mediated Ca^{2+} signaling was further confirmed by whole-cell patch-clamp recordings. Cation substitution experiments showed that bFGF activated inward currents primarily involving Ca^{2+}. These and the associated conductance changes were significantly reduced by antisense/TRPC1 treatment and eliminated completely by pharmacological blockers of voltage-independent cation channels. TRPC1 has been proposed to be associated with store-operated Ca^{2+} influx (Liu et al., 2000; Vaca and Sampieri, 2002; Beech et al., 2003). However, the present data do not establish whether TRPC1 mediates store-operated or non-store-operated Ca^{2+} entry in response to bFGF/FGFR-1 signaling in NSC progeny. Besides a contribution attributable to Ca^{2+} release from the intracellular stores, other pathways are activated by bFGF/FGFR1 signaling (for review, see Vaccarino et al., 1999b; Cross and Claesson-Welsh, 2001). For example, stimulation of phospholipase C γ leads to the generation of DAG together with IP_3. DAG is known to stimulate Ca^{2+} influx through TRPC channels, in particular TRPC3, TRPC6, and TRPC7 (Hofmann et al., 1999; Clapham, 2003). In this regard, we show here that there was no effect of antisense/TRPC1 treatment on Ca_i^{2+} responses induced by OAG, which involve Ca^{2+} entry but not Ca^{2+} release from intracellular stores. The unmodified Ca^{2+} responses to OAG demonstrate that OAG-sensitive Ca^{2+} entry mechanisms do not involve TRPC1 channels. Furthermore, a previous study has shown that TRPC1 can heterotetramerize with other TRPCs expressed during brain development, forming complexes containing TRPC1/TRPC3/TRPC6 and TRPC1/TRPC4/TRPC5, giving rise to channels with different properties (Strübing et al., 2003). We have used RT-PCR and immunocytochemistry to detect the presence of TRPC channels other than TRPC1 in the embryonic rat telencephalon and in NSCs profiled *ex vivo* with flow cytometry. Interestingly, *TRPC5* mRNA expression displayed a differential distribution in the E13 telencephalon. It was detected in dissociates of the entire telencephalon and in the neuronal progenitor subpopulation but not in NSCs, which express TRPC1–4 and 6. These data exclude a possible interaction between TRPC1 and TRPC5 in the NSC. The absence of TRPC5 in NSCs may help to explain the *I–V* characteristics of bFGF-activated currents in

NSC-derived progeny, which differ from those described for heteromeric TRPC(1+5) and TRPC(1+3+5) channels (Strübing et al., 2003). Thus, our results do not exclude a possible involvement of other TRPC channels during NSC proliferation, cell lineage progression, and the development of the telencephalon. In this regard, it is likely that the other members of the TRPC family expressed by NSCs mediate the OAG-evoked Ca^{2+} responses recorded in NSC progeny. Future studies will address whether these channels are involved in bFGF/FGFR-1-mediated NSC proliferation.

In conclusion, our study indicates that TRPC1 plays a role in NSC proliferation by contributing to bFGF/FGFR-1-induced Ca^{2+} influx.

References

Antoniotti S, Lovisolo D, Fiorio Pla A, Munaron L (2002) Expression and functional role of bTRPC1 channels in native endothelial cells. FEBS Lett 510:189–195.

Beech DJ, Xu SZ, McHugh D, Flemming R (2003) TRPC1 store-operated cationic channel subunit. Cell Calcium 33:433–440.

Bezzerides VJ, Ramsey IS, Kotecha S, Greka A, Clapham DE (2004) Rapid vesicular translocation and insertion of TRP channels. Nat Cell Biol 6:709–720.

Brazer SC, Singh BB, Liu X, Swaim W, Ambudkar IS (2003) Caveolin-1 contributes to assembly of store-operated Ca^{2+} influx channels by regulating plasma membrane localization of TRPC1. J Biol Chem 278:27208–27215.

Chao TS, Byron KL, Lee KM, Villereal M, Rosner MR (1992) Activation of MAP kinases by calcium-dependent and calcium-independent pathways. Stimulation by thapsigargin and epidermal growth factor. J Biol Chem 267:19876–19883.

Clapham DE (2003) TRP channels as cellular sensors. Nature 426:517–524.

Cross MJ, Claesson-Welsh L (2001) FGF and VEGF function in angiogenesis: signalling pathways, biological responses and therapeutic inhibition. Trends Pharmacol Sci 22:201–207.

Dono R, Texido G, Dussel R, Ehmke H, Zeller R (1998) Impaired cerebral cortex development and blood pressure regulation in FGF-2-deficient mice. EMBO J 17:4213–4225.

Golovina VA, Platoshyn O, Bailey CL, Wang J, Limsuwan A, Sweeney M, Rubin LJ, Yuan JX (2001) Upregulated TRP and enhanced capacitative Ca^{2+} entry in human pulmonary artery myocytes during proliferation. Am J Physiol Heart Circ Physiol 280:H746–H755.

Hofmann T, Obukhov AG, Schaefer M, Harteneck C, Gudermann T, Schultz G (1999) Direct activation of human TRPC6 and TRPC3 channels by diacylglycerol. Nature 397:259–263.

Kao JP, Alderton JM, Tsien RY, Steinhardt RA (1990) Active involvement of Ca^{2+} in mitotic progression of Swiss 3T3 fibroblasts. J Cell Biol 111:183–196.

Kilkenny DM, Rocheleau JV, Price J, Reich MB, Miller GG (2003) c-Src regulation of fibroblast growth factor-induced proliferation in murine embryonic fibroblasts. J Biol Chem 278:17448–17454.

Kim SJ, Kim YS, Yuan JP, Petralia RS, Worley PF, Linden DJ (2003) Activation of the TRPC1 cation channel by metabotropic glutamate receptor mGluR1. Nature 426:285–291.

Korada S, Zheng W, Basilico C, Schwartz ML, Vaccarino FM (2002) Fibroblast growth factor 2 is necessary for the growth of glutamate projection neurons in the anterior neocortex. J Neurosci 22:863–875.

Li HS, Xu XZ, Montell C (1999) Activation of a TRPC3-dependent cation current through the neurotrophin BDNF. Neuron 24:261–273.

Liu X, Wang W, Singh BB, Lockwich T, Jadlowiec J, O'Connell B, Wellner R, Zhu MX, Ambudkar IS (2000) Trp1, a candidate protein for the store-operated Ca^{2+} influx mechanism in salivary gland cells. J Biol Chem 275:3403–3411.

Liu X, Groschner K, Ambudkar IS (2004) Distinct Ca^{2+}-permeable cation currents are activated by internal Ca^{2+}-store depletion in RBL-2H3 cells and human salivary gland cells, HSG and HSY. J Membr Biol 200:93–104.

Lockwich T, Singh BB, Liu X, Ambudkar IS (2001) Stabilization of cortical actin induces internalization of transient receptor potential 3 (Trp3)-associated caveolar Ca^{2+} signaling complex and loss of Ca^{2+} influx without disruption of Trp3-inositol trisphosphate receptor association. J Biol Chem 276:42401–42408.

Lockwich TP, Liu X, Singh BB, Jadlowiec J, Weiland S, Ambudkar IS (2000) Assembly of Trp1 in a signaling complex associated with caveolin-scaffolding lipid raft domains. J Biol Chem 275:11934–11942.

Ma W, Maric D, Li BS, Hu Q, Andreadis JD, Grant GM, Liu QY, Shaffer KM, Chang YH, Zhang L, Pancrazio JJ, Pant HC, Stenger DA, Barker JL (2000) Acetylcholine stimulates cortical precursor cell proliferation in vitro via muscarinic receptor activation and MAP kinase phosphorylation. Eur J Neurosci 12:1227–1240.

Maric D, Maric I, Ma W, Lahojuji F, Somogyi R, Wen X, Sieghart W, Fritschy JM, Barker JL (1997) Anatomical gradients in proliferation and differentiation of embryonic rat CNS accessed by buoyant density fractionation: alpha 3, beta 3 and gamma 2 $GABA_A$ receptor subunit coexpression by post-mitotic neocortical neurons correlates directly with cell buoyancy. Eur J Neurosci 9:507–522.

Maric D, Maric I, Barker JL (1998a) Buoyant density gradient fractionation and flow cytometric analysis of embryonic rat cortical neurons and progenitor cells. Methods 16:247–259.

Maric D, Maric I, Smith SV, Serafini R, Hu Q, Barker JL (1998b) Potentiometric study of resting potential, contributing K^+ channels and the onset of Na^+ channel excitability in embryonic rat cortical cells. Eur J Neurosci 10:2532–2546.

Maric D, Maric I, Barker JL (2000a) Developmental changes in cell calcium homeostasis during neurogenesis of the embryonic rat cerebral cortex. Cereb Cortex 10:561–573.

Maric D, Maric I, Chang YH, Barker JL (2000b) Stereotypical physiological properties emerge during early neuronal and glial lineage development in the embryonic rat neocortex. Cereb Cortex 10:729–747.

Maric D, Maric I, Barker JL (2000c) Dual video microscopic imaging of membrane potential and cytosolic calcium of immunoidentified embryonic rat cortical cells. Methods 21:335–347.

Maric D, Maric I, Chang YH, Barker JL (2003) Prospective cell sorting of embryonic rat neural stem cells and neuronal and glial progenitors reveals selective effects of basic fibroblast growth factor and epidermal growth factor on self-renewal and differentiation. J Neurosci 23:240–251.

Orr-Urtreger A, Givol D, Yayon A, Yarden Y, Lonai P (1991) Developmental expression of two murine fibroblast growth factor receptors, flg and bek. Development 113:1419–1434.

Ortega S, Ittmann M, Tsang SH, Ehrlich M, Basilico C (1998) Neuronal defects and delayed wound healing in mice lacking fibroblast growth factor 2. Proc Natl Acad Sci USA 95:5672–5677.

Pitt BR, Weng W, Steve AR, Blakely RD, Reynolds I, Davies P (1994) Serotonin increases DNA synthesis in rat proximal and distal pulmonary vascular smooth muscle cells in culture. Am J Physiol 266:L178–L186.

Raballo R, Rhee J, Lyn-Cook R, Leckman JF, Schwartz ML, Vaccarino FM (2000) Basic fibroblast growth factor (Fgf2) is necessary for cell proliferation and neurogenesis in the developing cerebral cortex. J Neurosci 20:5012–5023.

Reilly JF, Mickey G, Maher PA (2000) Association of fibroblast growth factor receptor 1 with the adaptor protein Grb14. Characterization of a new receptor binding partner. J Biol Chem 275:7771–7778.

Rosado JA, Sage SO (2001) Activation of store-mediated calcium entry by secretion-like coupling between the inositol 1,4,5-trisphosphate receptor type II and human transient receptor potential (hTrp1) channels in human platelets. Biochem J 356:191–198.

Shin DM, Korada S, Raballo R, Shashikant CS, Simeone A, Taylor JR, Vaccarino F (2004) Loss of glutamatergic pyramidal neurons in frontal and temporal cortex resulting from attenuation of FGFR1 signaling is associated with spontaneous hyperactivity in mice. J Neurosci 24:2247–2258.

Singh BB, Zheng C, Liu X, Lockwich T, Liao D, Zhu MX, Birnbaumer L, Ambudkar IS (2001) Trp1-dependent enhancement of salivary gland fluid secretion: role of store-operated calcium entry. FASEB J 15:1652–1654.

Singh BB, Liu X, Tang J, Zhu MX, Ambudkar IS (2002) Calmodulin regulates Ca^{2+}-dependent feedback inhibition of store-operated Ca^{2+} influx by interaction with a site in the C terminus of TrpC1. Mol Cell 9:739–750.

Strübing C, Krapivinsky G, Krapivinsky L, Clapham DE (2003) Formation of novel TRPC channels by complex subunit interactions in embryonic brain. J Biol Chem 278:39014–39019.

Sweeney M, Yu Y, Platoshyn O, Zhang S, McDaniel SS, Yuan JX (2002a) Inhibition of endogenous TRP1 decreases capacitative Ca^{2+} entry and attenuates pulmonary artery smooth muscle cell proliferation. Am J Physiol Lung Cell Mol Physiol 283:L144–L155.

Sweeney M, McDaniel SS, Platoshyn O, Zhang S, Yu Y, Lapp BR, Zhao Y, Thistlethwaite PA, Yuan JX (2002b) Role of capacitative Ca^{2+} entry in bronchial contraction and remodeling. J Appl Physiol 92:1594–1602.

Vaca L, Sampieri A (2002) Calmodulin modulates the delay period between release of calcium from internal stores and activation of calcium influx via endogenous TRP1 channels. J Biol Chem 277:42178–42187.

Vaccarino FM, Schwartz ML, Hartigan D, Leckman JF (1995) Basic fibroblast growth factor increases the number of excitatory neurons containing glutamate in the cerebral cortex. Cereb Cortex 5:64–78.

Vaccarino FM, Schwartz ML, Raballo R, Nilsen J, Rhee J, Zhou M, Doetschman T, Coffin JD, Wyland JJ, Hung YT (1999a) Changes in cerebral cortex size are governed by fibroblast growth factor during embryogenesis. Nat Neurosci 2:246–253.

Vaccarino FM, Schwartz ML, Raballo R, Rhee J, Lyn-Cook R (1999b) Fibroblast growth factor signaling regulates growth and morphogenesis at multiple steps during brain development. Curr Top Dev Biol 46:179–200.

Wang W, O'Connell B, Dykeman R, Sakai T, Delporte C, Swaim W, Zhu X, Birnbaumer L, Ambudkar IS (1999) Cloning of Trp1beta isoform from rat brain: immunodetection and localization of the endogenous Trp1 protein. Am J Physiol 276:C969–C979.

Webb SE, Miller AL (2003) Calcium signalling during embryonic development. Nat Rev Mol Cell Biol 4:539–551.

Yuan JP, Kiselyov K, Shin DM, Chen J, Shcheynikov N, Kang SH, Dehoff MH, Schwarz MK, Seeburg PH, Muallem S, Worley PF (2003) Homer binds TRPC family channels and is required for gating of TRPC1 by IP_3 receptors. Cell 114:777–789.